Satellites quantify the spatial extent of cyanobacterial blooms across the United States at multiple scales.

Blake A. Schaeffer[1*], Erin Urquhart[2], Megan Coffer[3], Wilson Salls[1], Richard P. Stumpf[4], Keith A. Loftin[5], P. Jeremy Werdell[6]

1. Office of Research and Development, US Environmental Protection Agency, 109 TW Alexander Drive, Durham, NC 27709,
2. Science Systems and Applications, Inc., Ocean Ecology Laboratory, NASA Goddard Space Flight Center, Greenbelt, MD, USA
3. Oak Ridge Institute for Science and Education (ORISE), US Environmental Protection Agency, 109 TW Alexander Drive, Durham, NC 27709
4. National Oceanic and Atmospheric Administration, National Centers for Coastal Ocean Science, 1305 East-West Highway code N/SCI1, Silver Spring, MD 20910
5. US Geological Survey, Organic Geochemistry Research Laboratory, Kansas Water Science Center, 1217 Biltmore Drive, Lawrence, KS 66049
6. Ocean Ecology Laboratory, NASA Goddard Space Flight Center, 8800 Greenbelt Road, Greenbelt, MD 20771

*Corresponding author: schaeffer.blake@epa.gov
Target journal: Ecological Indicators

Highlights:

- National spatial extent increased from 2017–2020 but did not change from 2008–2011
- Satellite measures were available for over 2,000 larger lakes and reservoirs
- Cyanobacterial spatial extent changes were dependent on spatial and temporal scales
- Region, state, and lake scales show complex patterns of change in the U.S.
- A decline, or no change, does not indicate a lack of cyanobacteria-related issues

Abstract

Previous studies suggest that cyanobacterial harmful algal bloom (cyanoHAB) frequency, extent, and magnitude have increased globally over the past few decades. However, there is little quantitative capability available to assess these metrics of cyanoHABs across broad geographic scales and at regular intervals. Here, the spatial extent was quantified from a cyanobacteria algorithm applied to two European Space Agency satellite platforms— the MEdium Resolution Imaging Spectrometer (MERIS) onboard Envisat and the Ocean Land Colour Instrument (OLCI) onboard Sentinel-3. CyanoHAB spatial extent was defined for each geographic area as the percentage of valid satellite pixels that exhibited detectable cyanobacteria above the detection limit of the satellite sensor. This study quantified cyanoHAB spatial extent for over 2,000 large lakes and reservoirs across the contiguous United States (CONUS) during two time periods: 2008–2011 via MERIS and 2017–2020 via OLCI when cloud-, ice-, and snow-free imagery was available. Where approximately 56% of resolvable lakes were glaciated; and 13% of resolvable lakes represented headwater, isolated, or terminal lakes while the remaining lakes were primarily drainage lakes. Results were summarized at the national-, regional-, state-, and lake-scale, where

regions were defined as nine regions which represent climatically consistent states. As measured by satellite, changes in national cyanoHAB extent did have a strong increase of 6.9% from 2017–2020 (|Kendall's *tau* (τ)| = 0.56; *gamma* (*γ*) = 2.87 years), but had negligible change (|τ| = 0.03) from 2008–2011. Two of the nine regions had moderate ($0.3 \leq |\tau| < 0.5$) increases in spatial extent from 2017–2020, and eight of nine regions had negligible ($|\tau| < 0.2$) change from 2008–2011. Twelve states had a strong or moderate increase from 2017–2020 ($|\tau| \geq 0.3$), where only one state with a moderate increase and two states with a moderate decrease from 2008–2011. A decline, or no change, in cyanoHAB surface area extent did not indicate a lack of issues related to cyanoHABs. Sensitivity results of randomly omitted daily CONUS scenes confirm that even with reduced data availability during a short four-year temporal assessment, the direction and strength of the changes in spatial extent remained consistent. We present the first set of national maps of freshwater cyanoHAB spatial extent across CONUS and demonstrate an approach for quantifying past and future changes at multiple spatial scales. Results presented here provide water quality managers information regarding current cyanoHAB spatial extent and quantify rates of change.

Keywords: Harmful Algal Blooms; Cyanobacteria; Satellite Remote Sensing; Water Quality; Lakes, Spatial Extent

1. Introduction

Cyanobacterial harmful algal blooms (cyanoHABs), as defined in Smayda (1997), have adverse impacts on the environment, animal, and human health (Paerl and Huisman, 2009; Kahru and Elmgren, 2014; Matthews, 2014; Wynne and Stumpf, 2015; De Bakker et al., 2017; Svirčev et al., 2017) and have been found throughout the United States (Loftin et al., 2016). CyanoHABs may produce toxins and cause food web alterations, nuisance odors, hypoxia, and increased turbidity, leading to decreased light penetration in lake ecosystems (Kutser et al., 2006; Paerl et al., 2011; Michalak et al., 2013). While it is suggested that there has been an "apparent global increase" (Hallegraeff, 1993) in cyanoHABs over the past few decades (Paerl and Paul, 2012; Taranu et al., 2015), there is a lack of data available to quantify an increase of spatial extent and temporal changes of these events on a global or continental scale (Chorus and Bartram, 1999).

The limited information on the occurrence and spatial extent of cyanoHABs in United States lakes poses a future risk to the environment and public health. Assessment methods are needed to provide timely information in regions experiencing cyanoHABs as well as regions not yet impacted by blooms. Information on cyanoHAB location and extent is needed for routine monitoring and management of water quality and resources at the state level (Suter, 2007).

Many studies have used field, laboratory, and simulation models to quantify spatio-temporal changes in inland cyanobacterial blooms (Komatsu et al., 2007; Paerl and Huisman, 2008; Paerl and Huisman, 2009; Elliott, 2010; Deng et al., 2014). However, these studies often focus on a single, relatively large system (Verschuren et al., 2002; Chen et al., 2003; Duan et al., 2009; Kahru and Elmgren, 2014), making it difficult to generalize results to multiple lakes at the sub-continental scale (Li and He, 2014). Changes in cyanoHABs over time are often poorly resolved due to the lack of historical field data and comparable analytical approaches over similar spatial and temporal scales. Multi-scale assessments that are timely, standardized, and cost-effective are needed to better evaluate water quality, biological integrity, and management actions on local, regional, and national scales. Remote sensing offers a capability that provides an additional line of scientific evidence to help guide and complement field efforts and take another

step toward a more comprehensive means of assessment for the parameters that satellites can measure.

Satellite remote sensing can be used to effectively quantify cyanoHAB temporal frequency (Clark et al., 2017; Coffer et al., 2021a), spatial extent (Matthews, 2014; Urquhart et al., 2017), magnitude (Mishra et al., 2019), and lake occurrence (Coffer et al., 2020) on a routine basis for multiple waterbodies when sufficient cloud-, ice-, and snow-free scenes are available. Investigators have started using remotely sensed data to explore temporal and spatial changes in cyanoHABs across lakes and coastal systems at high spatial and temporal resolutions (Duan et al., 2009; Gómez et al., 2011; Kahru and Elmgren, 2014; Matthews and Odermatt, 2015; Palmer et al., 2015a; Wynne and Stumpf, 2015; Kahru et al., 2016). . Recently, Ho et al., (2019) used three decades of imagery from the NASA/USGS Landsat 5 satellite to determine long-term trends in summertime phytoplankton blooms in 71 large global lakes. Coffer et al. (2021b) used imagery from ESA's Ocean and Land Colour Instrument (OLCI) to analyze short-term changes from 2016-2020 in cyanobacterial abundance at drinking water sources across the United States. However, none of these studies have specifically quantified the change in spatial extent of cyanoHABs with all United States resolvable lakes at different scales.

Here, we develop the first available estimates of satellite-derived cyanoHAB spatial extent across the contiguous United States (CONUS) at the national-, regional-, state-, and lake-scales using eight years of satellite data spanning 2008 through 2011 and 2017 through 2020. The analysis of drivers was beyond the scope of this effort and has been reported elsewhere (Myer et al., 2020; Iiames et al., 2021). This work builds upon Urquhart et al. (2017) in which spatial extent was analyzed for the states of California, Florida, and Ohio from 2008 through 2011 using data from ESA's MERIS satellite sensor. In February 2016, ESA's Copernicus Sentinel-3A OLCI sensor was launched followed by Sentinel-3B in April 2018, both of which are functionally comparable to MERIS. Quantification of spatial extent for 2017 through 2020 using data from OLCI is provided here in the main manuscript as a current-day demonstration while supplemental material includes results from MERIS spanning 2008–2011. This study addressed the following research objectives: (1) quantify the spatial extent of satellite detected cyanoHABs at the national-, regional-, state-, and lake-scales from 2017–2020 and 2008–2011; (2) quantify the short-term change in spatial extent at the national-, regional-, and state-scales from 2017–2020 and 2008–2011; and (3) use cross validation to assess the robustness of observed short-term changes in cyanoHAB spatial extent.

2. Materials and methods

2.1. Satellite observations

The CI_{cyano} was calculated using a spectral shape algorithm initially described by Wynne et al. (2008), then revised and updated by Lunetta et al. (2015) based on new conditions from Matthews et al. (2012). A detailed description of the algorithm evolution is described in Section 2.1 of Coffer et al. (2020). Briefly, spectral bands centered at 665 nanometers (nm), 681 nm, and 709 nm are used to assess cyanobacterial bloom biomass, and those centered at 620 nm, 665 nm, and 681 nm are used as exclusion criteria to prevent the quantification of non-cyanobacterial blooms. Throughout this study, a pixel is classified as a cyanobacterial detection if the CI_{cyano} algorithm returns any detectable value ($CI_{cyano} > 0.0001$), indicating cyanobacteria in concentrations above the detection limit of the sensor.

Extensive field validation of the CI_{cyano} algorithm was previously demonstrated across Ohio, Florida, Rhode Island, Massachusetts, New Hampshire, Vermont, Connecticut, and Maine (Lunetta et al., 2015; Tomlinson et al., 2016). Additionally, Lunetta et al. (2015), revised by Clark et al. (2017), found good association between MERIS-derived CI_{cyano} values and corresponding *in situ* cyanoHAB abundance values (cells mL^{-1}; mean absolute percentage error = 28.6%). Validation of CI_{cyano} via a mobile device application performance test showed good correspondence in Oregon, California, Idaho, New Jersey, New York, Nevada, Utah, and Vermont with 25 historical health advisories (Schaeffer et al., 2018). The CI_{cyano} algorithm has also been used for guiding health advisories issued in Utah (Utah DEQ, 2018b, a), Wyoming (Wyoming DEQ, 2018a, b, c, 2019h, g, f, e, c, b, a, d), and New York (Schellhammer, 2019). Recently, CI_{cyano} algorithm performance was validated across CONUS lakes by evaluating the agreement between satellite observations and previously established ecological patterns, where cyanobacterial followed the well-known temporal pattern of freshwater blooms (Coffer et al., 2020). The algorithm has also been validated using state reported toxin data (84% overall agreement; Mishra et al., 2021), state reported events and advisories (73% overall agreement; Whitman et al., In Press), chlorophyll-a from the Water Quality Portal (60% mean absolute error; Seegers et al., 2021), and with visual observations from the fourth Unregulated Contaminant Monitoring Rule of algal bloom presence and absence near drinking water intakes (94% overall agreement; Coffer et al., 2021b). While CI_{cyano} has been predominantly used in the United States, it has also been demonstrated in the Caspian Sea (Moradi, 2014), Lake Balaton, Hungary (Palmer et al., 2015b), and Lakes Taihu and Chaohu, China (Jin et al., 2017).

A conceptual representation of the methods described in Sections 2.1 through 2.4 is provided in Fig. 1. Weekly satellite data were retrieved over CONUS from the OLCI sensor spanning January 2017 through December 2020 at a spatial resolution of 300 m (Seegers et al., 2021). Additionally, archived weekly satellite data were obtained over CONUS from the functionally similar MERIS sensor onboard the Envisat satellite for January 2008 through December 2011. While the MERIS sensor was intermittently available for CONUS from 2002 through 2007, continuous, full-resolution data were only available for CONUS between 2008 and 2012. In April 2012, the Envisat mission ended after loss of communication with the satellite, and no comparable sensor was available until Sentinel-3A was launched in 2016. MERIS and OLCI data were first obtained by NASA from ESA through a data sharing agreement and were then processed by the NASA Ocean Biology Processing Group (OBPG; https://oceancolor.gsfc.nasa.gov/projects/cyan/) using their standard satellite ocean color software package (l2gen; distributed publicly within the SeaWiFS Data Analysis System, SeaDAS, http://seadas.gsfc.nasa.gov) and a Shuttle Radar Topography Mission (SRTM)-derived 60-m land mask with updates to include missing lakes and reservoirs in Rhode Island and Massachusetts (Urquhart and Schaeffer, 2020). The SRTM land mask and SeaDAS processing are static in relation to waterbody size and did not account for periods of drought or flood during the study period. Flags to indicate potential contamination due to cloud, cloud shadow, and adjacency effects from neighboring land pixels, and to identify snow- or ice-covered waterbodies, were also applied (Wynne et al., 2018; Urquhart and Schaeffer, 2020). Therefore, these quality flags mask and exclude land contaminated pixels.

NASA OBPG merged Sentinel-3A and Sentinel-3B into the processing stream beginning May 15, 2018. Sentinel-3 satellites have the same orbits with Sentinel-3B 140° out of phase with Sentinel-3A, effectively doubling the number of observations at any given location. To avoid potentially erroneous change detection results due to increased observations from the inclusion of Sentinel-3B, daily observations within the Sentinel-3A orbital path were retained and those outside

the Sentinel-3A orbital path were removed. Orbital prediction files were accessed as shapefiles from EUMETSAT (access date November 21, 2021, https://www.eumetsat.int/s3a-3b-orbit-predictions-available). Daily flagging removed Sentinel-3B observations except where there was orbital path overlap on the same day, as the merged Sentinel-3 product is processed to yield the maximum value between the two sensors in the case of same-day overlap. In those cases, the difference between the two sensors was assumed to be minimal as collection times were nearly contemporaneous (within approximately 20–45 minutes). Therefore, all results were considered to be only from Sentinel-3A except for a specific test to demonstrate the effect of merging Sentinel-3A and -3B in section 3.6.

For each week spanning the 2008-2011 and 2017-2020 time periods, a spatial mosaic comprised of the 54 individual MERIS and OLCI tiles covering CONUS was generated using the maximum CI_{cyano} value for each pixel occurring during that 7-day period. Then, a one-pixel buffer along the land-water interface was applied and affected satellite pixels were flagged to prevent potential straylight and bottom reflectance contamination (Urquhart and Schaeffer, 2020). Lake water pixels were extracted using the National Hydrography Dataset Plus (NHDPlus) version 2.0 shapefiles (McKay et al., 2012) for each waterbody. All NHDPlus features categorized as lakes and reservoirs, referred to hereafter exclusively as lakes, were selected using the U.S. Environmental Protection Agency's 2012 National Lakes Assessment (NLA) site evaluation guidelines. Waterbodies classified as intermittent, estuarine, rivers, streams, or ponds, or with a surface area < 1 ha were excluded from further analysis based on NLA criteria. The categorization of lakes, based on NHDPlus, included coastal lagoon systems. Lakes in the NDHPlus shapefile with a minimum of three water pixel remaining were included and considered MERIS/OLCI resolvable lakes. A total of 2,192 NHDPlus waterbodies remained and were included in this study. The Great Lakes were excluded from this study, since other programs, such as the NOAA Lake Erie HAB Forecast System, already focus on these lakes (Stumpf et al., 2012; Wynne and Stumpf, 2015). Water remaining after land exclusion is here termed resolvable water. Total resolvable water area (km^2)—the area considered for analysis—was calculated as the number of resolvable water pixels multiplied by the spatial resolution (300 m × 300 m) of the MERIS and OLCI sensors (Eq. 1).

$$Water\ area\ (km^2) = n\ of\ valid\ pixels\ \times 0.09\ km^2 \quad (1)$$

Each 300-m satellite pixel in a weekly CONUS map represents a maximum cyanobacteria index (CI_{cyano}) value retrieved for that week.

Approximately 56% of the 2,192 NHDPlus resolvable lakes were glaciated. Thirteen percent of resolvable lakes represented headwater, isolated, or terminal lakes while the majority of lakes were drainage lakes (Cheruvelil et al., 2021; Smith et al., 2021). Dammed lakes accounted for 13% and over 99% of the resolvable lakes were classified as a lake defined in NHDPlus as a standing body of water with a predominantly natural shoreline surrounded by land, where <1% were classified as reservoir defined as a constructed basin formed to contain water. Most resolvable lakes were located within the Eastern Temperate Forest (39.5%), Northern Forest (22.8%), and Great Plains (20.8%) ecoregions. Ecoregions were defined as unique compositions of biotic and abiotic factors such as minerology, soil type, vegetation, climate, land use and hydrology that impact ecosystem quality and integrity (Omernik, 1995; Omernik and Griffith, 2014). There were 8.7% of lakes were in the Northwestern forested mountains, 4.7% in the North American Desert,

1.9 % in the Mediterranean California, 1.0 % in the Marine West Coast Forest, and in 0.5% in the Tropical Wet Forest and Temperate Sierras ecoregions.

2.2. Computing cyanobacterial spatial extent

The categorical approach applied here to CI_{cyano} results provided a simple binary response of non-detection or detection of cyanoHABs, thereby reducing the need for absolute accuracy on concentration from the CI_{cyano} algorithm, similar to Coffer et al (2020; 2021a). Weekly data (Sunday through Saturday) generated by NASA OBPG were aggregated into monthly composites containing average CI_{cyano} values for each pixel; the final day of the seven-day composite (Saturday) determined which month the weekly composite was allocated. Then, for each monthly composite, cyanobacterial spatial extent was calculated as the percentage of valid water pixels—that is, resolvable water pixels free of clouds or other quality flags—with cyanobacteria detection (Eq. 2).

$$Spatial\ extent\ (\%) = \frac{n\ of\ pixels\ with\ detectable\ CI_{cyano}}{n\ of\ valid\ pixels} \times 100\% \quad (2)$$

Spatial extent was also computed for each individual lake, state, and region by cropping national monthly composites to each respective boundary. Regions were defined by the National Center for Environmental Information (Karl and Koss, 1984) as nine climatically consistent regions across CONUS (Fig. S1). In the example for an individual lake shown in Figure 2, there were 23 satellite pixels (2.07 km^2) that were resolvable, 18 (1.62 km^2) of which were valid (i.e., not quality flagged). Of those 18 valid satellite pixels, 9 satellite pixels (0.81 km^2) were above the detection limit of the sensor and thus were considered cyanobacterial bloom pixels, yielding a cyanoHAB spatial extent value of 50%. When summarizing across a year or an entire satellite mission time period (2017–2020 or 2008–2011), spatial extent was calculated as the median of all monthly spatial extent values within that period.

2.3. Statistical methods and change assessment

Temporal changes of spatial extent were estimated at the national-, regional-, and state- scales. A rank-based nonparametric seasonal Mann-Kendall (MK) statistic (Kendall, 1938; Mann, 1945) was applied to monthly spatial extents to identify changes in cyanoHAB surface area extent. The seasonal MK test is a modification of the Kendall test for change that allows for seasonality, heterogeneity, and serial dependence in observations (Hirsch and Slack, 1984). The seasonal Kendall slope estimator (Hirsch et al., 1982), an extension of the Theil-Sen slope (Sen, 1968; Theil, 1992), was used to estimate the magnitude of change in the form of a slope (change per unit time). The seasonal Kendall slope estimator is nonparametric, computed as the median of all two-point slopes computed within each season, where our analysis defined seasons as individual months. Slopes are presented as the change in spatial extent over each satellite time period considered, either 2008–2011 or 2017–2020, along with the MK test statistic, Kendall's *tau* (τ). Kendall's τ (τ hereafter) indicates the strength of the monotonic changes (Akoglu, 2018; Helsel et al., 2020), with $|\tau| < 0.2$, $0.2 \leq |\tau| < 0.3$, $0.3 \leq |\tau| < 0.5$, $|\tau| \geq 0.5$, respectively, indicating negligible, weak, moderate, and strong changes over time as describe in Cohen (1988).

As an additional statistic to measure the strength of observed changes, the effect size metric *gamma* (γ) was computed. The γ statistic quantifies the number of observations needed for an observed change to be sustained despite residual variability in the data (Eq. 3). Since the time series considered for change detection both spanned four years (MERIS from 2008-2011, OLCI

from 2016-2020), γ is presented here in units of years, providing insight regarding how long the time series must be to increase confidence in an observed change; if γ is less than the time period of observations, the strength of the observed change exceeds residual variability in the data. The γ statistic has been presented in several environmental studies to quantify the number of years of observations needed to increase confidence in an observed trend: Urquhart et al. (2017) observed trends in cyanobacteria spatial extent for the states of Florida and California; Coffer et al. (2021b) assessed trends in cyanobacterial frequency at drinking water sources across CONUS; Coffer and Hestir (2019) evaluated changes in carbon storage and environmental conditions at Arctic wetlands; and Henson et al. (2010) detected changes in ocean chlorophyll and productivity globally .

$$\gamma = \frac{\sqrt{\frac{\sum_1^n (y-\hat{y})^2}{n-1}}}{|m|} \quad (3)$$

where n is the sample size, $\hat{y}$ is the residual of y, and m is the seasonal Kendall slope estimator.

As mentioned in Section 2.1, Sentinel-3A observations were retained using the orbital path of the sensor; however, state-scale cyanoHAB spatial extent was also computed using observations from both Sentinel-3A and -3B to assess the effect of increased observations on trend results. Increased temporal coverage due to the inclusion of Sentinel-3B increases the opportunity to record higher cyanoHAB spatial extents since methods used in this study retained the maximum CI_{cyano} value for each weekly composite. The effect of increased temporal coverage was tested by comparing Kendall's τ and the Kendall slope estimator for state-scale results computed using just Sentinel-3A and using combined Sentinel-3A and -3B. Resulting change assessment statistics were compared using the non-parametric Mann-Whitney U test (Wilcoxon, 1945; Mann and Whitney, 1947). Results of the Mann-Whitney U test were further distilled into an effect size following the Glass (1966) formulation of rank-biserial correlation (r_{rb}) which was then also classified according to Cohen (1988) where $0.1 \leq |r_{rb}| < 0.3$ indicates a small difference between samples, $0.3 \leq |r_{rb}| < 0.5$ indicates a moderate difference, and $|r_{rb}| \geq 0.5$ indicates a large difference. All data were processed and analyzed using R statistical software (R Core Team, 2015) and the *rkt* package was used for change assessment (Marchetto, 2017).

2.4 Sensitivity to missing observations

Observations over short time periods, such as 4-year intervals in this study, may be influenced by inter-annual variability, episodic bloom events, and data availability due to cloud cover. Therefore, we tested the robustness of our change assessment by randomly omitting weekly satellite composites prior to monthly aggregation to demonstrate the stability of change results at the national- and state-scales. For each year spanning 2017–2020, 10, 20, and 30% of weekly satellite composites were randomly omitted without replacement and spatial extent was recomputed. For each incremental increase in data omission, a new subset of weekly composites was excluded. Data omission was replicated ten times and average spatial extent was retained to account for sampling variability. Then, the seasonal MK test was reassessed, and the resulting Kendall τ test statistic was demonstrated under increased data exclusion.

3. Results

3.1 Resolvable lakes and water area

There were 2,192 NHDPlus lakes that were resolvable with 300-m MERIS/OLCI imagery, which comprise a median of 110,793 km^2 of resolvable surface water area across the 2017–2020 time period, when accounting for missing data due to clouds, snow, and ice as well as invalid data due to the land/water boundary (Fig. 3). The sum total of resolvable area time series across CONUS had a minimum of 47,833 km^2 and maximum of 11,4361 km^2 (Fig. S2). Spatially, all contiguous states, apart from Delaware and West Virginia, had MERIS/OLCI resolvable lakes containing at least three non-land-adjacent satellite pixels. Individual state lake counts ranged from three to five lakes in Connecticut (CT), Maryland (MD), and Rhode Island (RI), to 393 lakes in Minnesota (MN). The median surface water area resolved by OLCI for each state from 2017–2020 ranged from 5 km^2 in CT to 14,454 km^2 in MN.

3.2 National-scale spatial extent

The mean monthly cyanoHAB spatial extent for CONUS is shown for 2017–2020 in Fig. 4 and 2008–2011 in Fig. S3. From 2017–2020, national-scale spatial extent values ranged from a minimum of 17.9% to a maximum of 41.6%, with a median value of 30.7%. CyanoHAB spatial extent had a strong (τ = 0.56, γ = 2.87 years) increase of 6.92% over the time period considered, as the seasonal Kendall slope estimator indicated an increase from 26% at the beginning of 2017 to 33% by the end of 2020. From 2008–2011, cyanoHAB spatial extent had a negligible (τ = -0.03) decrease of -0.7%. As expected, the pattern of observed mean monthly cyanoHAB spatial extent was strongly phased with summer and autumn months, with maximum spatial extent occurring during late summer or early autumn (Fig. 4). The shapes of the seasonal periodicity were somewhat bimodal, with smaller peaks in late winter or spring preceding the summer maxima. Each summer peak was followed by a general decrease in late autumn, and the minimum spatial extent occurred in winter each year.

3.3 Regional-scale spatial extent

From 2017–2020, OLCI imagery indicated that all regions increased in cyanobacterial spatial extent, although the strength of these changes varied (Table 1). In the Northeast, Southwest, and West regions, spatial extent had weak ($0.2 \leq |\tau| < 0.3$) increases of 10.8%, 1.76%, and 3.88% respectively, while the South and Southeast regions had moderate ($0.3 \leq |\tau| < 0.5$) increases of 8.58% and 10.93%, respectively. Spatial extent in the Northwest, Northwest Rockies and Plains, Ohio Valley, and Upper Midwest regions exhibited negligible ($|\tau| < 0.2$) changes from 2017–2020. OLCI period γ ranged from 3.55 to 17.22 years, with exception of the Ohio Valley, which required over 100 years for the observed trend to outweigh variability in the data. From 2008–2011, MERIS imagery indicated that nearly all regions had negligible ($|\tau| < 0.2$) changes in the monthly spatial extent, the only exception being the Southwest region where spatial extent decreased by -4.52% over the period considered with a weak τ of -0.25 (Table S1). MERIS period γ ranged from 3.98 to 49.14 years.

3.4 State-scale spatial extent

From 2017–2020, cyanobacterial spatial extent values and standard deviations tended toward lower values with no states falling in the highest quarter of potential values (76-100% spatial extent), and 26 states falling in the lowest quarter (0-25% spatial extent; Fig. 5A). Eight states had a median spatial extent at or above 50%: 50% in Mississippi, 52% in Rhode Island, 56% in Maryland, 59% in North Carolina, 61% in Wisconsin, 66% in Ohio, 68% in Oregon, and 71% in Florida. Spatial extent variability was expressed in terms of standard deviation and tended to be highest in states with either high or low resolvable water area, such as in the Upper Midwest states

and the Northeast states (Fig. 5B). It is important to remember that in the northern latitude states, spatial extent can be biased toward higher values due to missing data from snow and ice masking during the winter. However, Coffer et al. (2021a, see Table 1) found only negligible to small effect sizes in cyanobacterial bloom frequency caused by limited wintertime data in most regions (Cohen's d between 0.00 and 0.12) with exceptions in the Northwest Rockies and Plains region, which was largely biased by the exclusion of wintertime data (Cohen's d = 0.53), and the Ohio Valley and Southeast regions, which were moderately biased (Cohen's d = 0.39 and 0.42, respectively).

From 2008–2011, state results were more evenly distributed across potential values, with six states falling in the highest quarter (76-100% spatial extent) and five states falling in the lowest quarter (0-25% spatial extent; Fig. S4A). States with median spatial extents in the highest quarter during 2008–2011 were Florida (91%), Oregon (83%), Arizona (81%), Mississippi (80%), and both Illinois and Ohio (75%). States with median spatial extents in the lowest quarter during 2008–2011 were Kentucky (10%), Alabama (13%), Tennessee (19%), South Carolina (23%) and Georgia (24%). Variation tended to be lower in the MERIS 2008–2011 dataset than the OLCI 2017–2020 dataset with the highest standard deviations in states that tended to have low resolvable water area (Fig. S4B).

The 2017–2020 change in spatial extent for each state is shown in Fig. 6 and Table 2. During 2017–2020, a strong increase ($|\tau| \geq 0.5$) in spatial extent was observed in New Jersey (24.75%) and Louisiana (17.8%) with γ of 2.84 and 3.14 years, respectively. In decreasing order of change in spatial extent over the time period, Massachusetts (42.38%), Florida (15.06%), New Hampshire (14.22%), Maine (10.73%), Michigan (10.5%), Oregon and Arizona both at 8.09%, Vermont (4.6%), South Dakota (4.01%), and Montana (3.98%) all increased with moderate strength ($0.3 \leq |\tau| < 0.5$) with γ between 2.33 and 8.07 years. Arkansas, Indiana, Iowa, Mississippi, North Dakota, Ohio, Pennsylvania, Tennessee, and Texas decreased; however, all had changes with negligible ($|\tau| < 0.2$) to weak ($0.2 \leq |\tau| < 0.3$) strengths with γ between 6.45 and 83.6 years.

The 2008–2011 changes in spatial extent for each state is shown in Fig. S5 and Table S2. Total MERIS 2008–2011 detectable spatial extent in Mississippi increased with moderate strength (τ = 0.33, γ = 5.45 years) by 12.91% over the time period considered. Conversely, Louisiana and Maine both exhibited a decrease in spatial extent by -16.89% and -12.87%, respectively, over the time period with moderate strength (τ = -0.31 and -0.37; γ = 4.53 and 8.84). All other states had either negligible or weak strength changes.

State spatial extent values were also quantified for each individual year during 2017–2020 using OLCI imagery (Fig. 7) and during 2008–2011 using MERIS imagery (Fig. S6), independent of change rate calculations. In 2017, only Wisconsin, Ohio, Oregon, Maryland, North Carolina, Mississippi, and Florida were in the third quarter and 30 states were in the lowest quarter of spatial extent. In 2018, Florida increased to the highest quarter and remained there until 2020. Illinois and Rhode Island entered the third quarter in 2018 and Rhode Island remained in this quarter through 2020. There was a 20% decrease in the number of states that remained in the lowest quarter from 2017 to 2020.

As supported by the analysis for 2008–2011, there were few changes in median annual spatial extent across the MERIS archive (Fig. S6). While there were eight states in the highest quarter in 2008, three of these dropped to the third quarter by 2009 and another dropped to the third quarter in 2010. Five states were in the highest quarter for the entire time period: Oregon, Arizona, Mississippi, Ohio, and Florida. Similarly, those in the lowest quarter remained relatively

stable throughout 2008–2011 as Kentucky, Tennessee, and Alabama consistently had low cyanobacterial spatial extent.

3.5 Lake-scale spatial extent

Each resolvable lake's spatial extent was quantified annually from 2017–2020 (Fig. 8; Fig. S7-S9) and 2008–2011 (Fig. S10-S13). The lakes in the lowest quarter with spatial extent 0-25% decreased across both time periods, from 1,305 lakes in 2017 to 990 lakes in 2020, and from 719 lakes in 2008 to 507 lakes in 2011. The count of lakes in the two middle quarters increased between 2017 and 2020, but remained relatively constant between 2008 and 2011. The lake count in the upper quarter increased across both time periods, from 448 to 519 lakes between 2017 and 2020, and from 670 to 978 lakes between 2008 and 2011. Monthly spatial extent variation from 2017 through 2020 was demonstrated for select lakes including Utah Lake, Lake Champlain, and Falls Lake (Fig. S14).

3.6 Effect of missing data and integration of Sentinel-3A and -3B

To test the influence of inter-annual variability in cloud cover and anomalous bloom events the strength of the spatial change results, we randomly omitted CONUS weekly composites throughout the 2017–2020 period prior to monthly binning. National- and state-scale changes were reassessed. Randomly omitting data changed the strength from strong to moderate at the national-scale (Table 3). When all data was used, cyanobacterial spatial extent across CONUS increased with high strength ($\tau = 0.56$). After omitting 10, 20, and 30% of weekly composites, the τ strength remained moderate ($\tau = 0.47, 0.44, 0.44$).

At the state-scale, results were notably similar across increasing levels of data removal (Table 3). Of the 46 CONUS states that contain at least one MERIS/OLCI resolvable lake, 35 states had τ values that were either consistently moderate to high ($|\tau| \geq 0.3$; bolded values) or negligible to low ($|\tau| < 0.3$; non-bolded values) across all levels of data omission. For several states, τ increased with increased data omission, causing some states to shift from low strength to moderate strength. For example, Rhode Island (RI) exhibited an increase in cyanobacteria spatial extent from 2017–2020 with weak strength ($\tau = 0.29$) when all data was used; however, after randomly omitting 10, 20, and 30% of weekly composites, τ increased in strength to 0.33, 0.39, and 0.33, although τ did not monotonically increase with increasing data omission. Only two states, Maine (ME) and Michigan (MI), shifted in strength where spatial extent increased moderately when all data was used but increased negligibly when 30% of weekly composites were randomly omitted.

To test the influence of integrating Sentinel-3B with Sentinel-3A as originally processed by NASA OBPG, seasonal Mann-Kendall statistics was reported for each CONUS state as a demonstration. Combined Sentinel-3A and -3B spatial extent from 2017–2020 (Table S3) had strong increases ($|\tau| \geq 0.5$) in spatial extent in New Jersey (NJ; 32.50%), Louisiana (LA; 25.18%), Michigan (MI; 13.64%), and South Dakota (SD; 5.58%). In decreasing order of change in spatial extent over the time period, Massachusetts (MA; 47.75%), Maine (ME; 22.79%), Florida (FL; 22.54%), Rhode Island (RI; 21.08%), New Hampshire (NH; 19.05%), Nevada (NV; 16.04%), Arizona (AZ; 10.44%), Oregon (OR; 10.11%), North Carolina (NC; 7.34%), Alabama (AL; 5.08%), Montana (MT; 4.96%), and California (CA; 3.88%) all increased with moderate strength ($0.3 \leq |\tau| < 0.5$). Only Indiana (IN), Iowa (IA), Mississippi (MS), North Dakota (ND), and Ohio (OH) decreased; however, all had changes with negligible ($|\tau| < 0.2$) to weak ($0.2 \leq |\tau| < 0.3$) strengths. Inclusion of the merged Sentinel-3A and -3B results increased all state spatial extent changes over time by an average of 3.72% ± 0.03%, but the Mann Whitney U test indicated that

these changes were not significantly different (U = 1318.5, $n_{1,2}$ = 48, r_{rb} = 0.25) when compared to results computed using only Sentinel-3A (Fig. S15). State-scale τ strengths were also not significantly different (U = 1329.5, $n_{1,2}$ = 48, r_{rb} = 0.26) when merged Sentinel-3A and -3B results were compared to results generated using only Sentinel-3A. Twenty-six states with a weak or negligible τ strength remained weak or negligible. Twelve states with moderate or strong τ strength remained moderate or strong. Only 8 of the 46 states changed from weak or negligible to moderate τ strength.

4 Discussion

Temporal changes in cyanoHAB spatial extent across CONUS for a period of 2017–2020 (Fig. 4) and 2008–2011 (Fig. S3) were evaluated. We provide the first national-, regional, state- and lake-scale maps of cyanoHAB spatial extent across CONUS, relevant to management decisions for states and local organizations. As measured by satellite, there was a strong increase in cyanoHAB spatial extent of 6.92% during 2017–2020, while we found no indication of a strong or moderate national-scale change during 2008–2011. A bimodal response with a peak in spring preceding a summer maximum is consistent with phytoplankton seasonal cycles (Winder and Cloern, 2010). The approximate 4-year temporal gap from 2012 to 2016 between MERIS and OLCI limited extrapolation of longer-term change assessment analysis.

While Ho et al. (2019) reported an overall global increase of freshwater phytoplankton blooms from 1984 to 2012, further separation of the seven United States lakes in their study revealed a mixed response. Six of the seven United States lakes considered by Ho et al. (2019) were included in this study. In Ho et al. (2019), improvements were seen in Clear lake, CA; no change was seen at Salton Sea Lake, CA, Winnebago Lake, WI, or Walker Lake, NV; and deterioration was seen in Great Salt Lake, UT, and Lake Okeechobee, FL. As Figs. 5 through 8 clearly indicate, sub-national variability is high across CONUS both spatially and temporally. Ignoring region-, state-, and lake-scale patterns to focus only on the national-scale result may mislead interpretations of cyanoHAB change and status in the United States. In addition, these changes may not be entirely due to natural or climatic influences, as there may be artificial treatments of these lakes such as various chemical methods (Jancula and Marsalek, 2011), physical or biological methods (Zhang et al., 2020), or even nutrient enrichment (Lin et al., 2021).

When spatial extent was scaled to regions, rates of change had mixed responses during the 2008–2011 (MERIS) time period and increased spatial extent during 2017–2020 (OLCI). Ho et al. (2019) reported that lake warming may be important for global freshwater phytoplankton blooms. El Niño Southern Oscillation patterns were similar for both the MERIS and OLCI time periods—La Niña occurring the first year, a switch from La Niña to El Niño the second year, a continuation of El Niño the third year to either La Niña in 2010 or normal conditions in 2019, and La Niña occurring the final year (NOAA, 2021). Lake temperature and precipitation have been found to be important drivers in many other cyanoHAB studies (Paerl and Paul, 2012; Ho and Michalak, 2019; Myer et al., 2020).

State-scale temporal frequency of cyanoHABs were previously reported for the OLCI and MERIS time periods (Coffer et al., 2021a). Briefly, the temporal frequency metric was computed as the percentage of weekly satellite composites exhibiting cyanobacterial presence also with a $CI_{cyano} > 0.0001$ relative to the total number of weekly satellite composites that contained a valid measurement. Generally, states with higher temporal frequency presented in Coffer et al. (2021a) had higher spatial extent in this study (Fig. 5 and S3), although this was not always a one-to-one relationship. It was expected that some locations will have events with both low and high temporal

frequency, and will occur across different proportions of spatial extent area. The state-scale standard deviations (Fig. 5B) are relatively small, which supports interannual stability and consistency amongst years in Figure 7.

From 2017–2020, there were 12 states that had a strong or moderate increase in cyanoHAB spatial extent (Fig. 6). For 2008–2011, there was only one state where the change assessment showed a moderate increase in spatial extent, and two states with a moderate decrease, with all other states having negligible or weak strength changes (Fig. S4). States that exhibited a decline or no change should not be considered as lacking cyanoHAB issues; for example, in Maine we see a decline in cyanoHAB extent during 2008–2011 and yet more than 75% of resolvable water area had detectable cyanoHABs during that time period (Fig. S3). Further, statistics are derived from a constrained period of four-year cycles and many of the γ values indicated that more than four years of data were needed for an observed change to be sustained given the residual variability in the data. These results are consistent with those from South Africa (Matthews, 2014), where findings show that the overall change in cyanoHAB coverage in 50 large waterbodies remained uncertain, with an approximately equal number of lakes significantly increasing and decreasing using MERIS data from 2002 to 2011. Similarly, Hallegraeff et al. (2021) found contrasting regional changes in the distribution of marine HAB events over time, after adjusting for regional variations in monitoring effort.

Comparing changes in cyanoHAB spatial extent with those presented for the states of Florida, Ohio, and California in Urquhart et al. (2017) reveals some minor differences attributed to modifications in the change assessment method used. Here we used spatial extent, expressed as percentage area bloom (%), instead of area bloom (km^2) used in the previous study. Use of percentage area bloom reduces pixel availability bias by dividing bloom area by resolvable water area instead of total water area. This captures the dynamic nature of clouds, snow, and ice on resolvable water area. Coffer et al (2021a) tested whether reduced observations from snow and ice biased results in regions with more snow and ice, given observations were more likely in warmer months when cyanoHABs were more likely to occur. That study reported most regions were unbiased, only with a large bias in the Northwest Rockies and Plains (Wilcoxon signed-rank effect size 0.53) and moderate biases for the Ohio Valley (effect size 0.39) and the Southeast (effect size 0.42) regions. Further, we used monthly mean of the weekly maximums rather than the monthly maximum of the weekly maximums for temporal analysis. Monthly means likely offer a better representation of cyanoHAB events over longer periods of time such as a month. Lastly, the spatial footprint of the Florida MERIS imagery now encompasses the entire state, including lakes that were omitted from the original analysis. However, NHDPlus rivers and streams are excluded, including the lower St. Johns River—a Florida river system that exhibited a strong statistical increase in cyanoHAB spatial extent during 2008–2011 in the original analysis. Florida and California show little difference in the direction and strength of their MK values between this study and Urquhart et al. (2017). The direction of change in spatial extent across Ohio's lakes was different (decreasing for Urquhart et al. study but increasing for this study between 2008–2011), but this was not surprising as the calculated changes in both analyses were small relative to the high variability in the datasets and the Urquhart et al. (2017) study did not include a snow and ice mask.

In the current study, spatial variability within lakes was consistent within a lake year-over-year. Therefore, variability is primarily due to spatial variation between lakes (Fig. 8 and S4-S10) and not due to temporal variation within lakes for both the MERIS and OLCI time periods. A similar pattern was demonstrated with national lake temporal frequency (Coffer et al., 2021a).

There was a noticeable shift in the number of lakes in the lowest quarter (0-25% cyanoHAB spatial extent) from the MERIS to OLCI time periods and this could be due to either sensor differences in the minimum detection limit or actual ecological changes.

As continuous, full resolution acquisitions across CONUS are only available for 2017–2020 and 2008–2011, the assessment results are limited by the short time interval with only four years of data from each sensor and may be influenced by climate, anomalous bloom events, and data availability due to cloud cover (Clark et al., 2017; Coffer et al., 2020). While four years is a short time period, evidence of change detection in this short time frame has been previously documented (Psilovikos et al., 2006; Kim et al., 2009; Coffer et al., 2021b). Sensitivity analysis results of randomly omitting daily CONUS scenes prior to temporal binning indicate that even with reducing data availability during a short four-year temporal assessment, the direction and strength of the changes in spatial extent remained consistent in states with moderate and strong τ values (Table 3).

The ongoing OLCI archive provides potential for longer-term assessment as the data record increases with time. Sentinel-3A data became available during the latter part of 2016, with the first full calendar year covered in 2017. NASA OBPG integrated Sentinel-3A and -3B into the processing stream beginning May 15, 2018. Sentinel-3C and -3D are scheduled for launch in 2024 and 2028, respectively. Spatial extent changes and τ strengths were not significantly different after the inclusion of the Sentinel-3B compared to only Sentinel-3A (Fig. S15). Satellite water quality long-term analyses have focused on transitioning from one satellite to the next satellite creating time series for spatially continuous ocean waters (Kahru et al., 2012; Mélin, 2016; Melin et al., 2017). The merging of Sentinel-3A and -3B as well as the future inclusion of Sentinel-3C and -3D fills temporal and spatial observations across spatially discontinuous inland systems at increasing data densities. However, influence of changing data densities across spatially discontinuous systems for long-term analysis is something that needs to be considered in future work.

While the ability to quantify changes in inland cyanoHABs at national, regional, state, and individual lake scales using satellite data was demonstrated here, it is important to note the operating boundaries of this work. First, the spatial resolution of the MERIS and OLCI satellite datasets is relatively low (300 m x 300 m), as becomes apparent when measuring nearshore pixels and when calculating the number of resolvable waterbodies across CONUS. Results are from a subset of the nation's lakes—specifically, larger freshwater lakes and reservoirs. Higher-resolution sensors such as those on Landsat-8 and Sentinel-2 may provide assessment for smaller waterbodies in the future as tailored cyanoHAB detection methods for those instruments mature. Another potential limitation occurs when a cyanoHAB is mixed vertically in the water column. Wind and wave action impact the detection via satellites by mixing the biomass vertically in the water column or horizontally either along the shoreline or into the center of the lake (Rogalus and Watzin, 2008; Cuypers et al., 2011; Gonzalez-Piana et al., 2018). These physical forces impact the ability of the satellite to detection biomass (Kutser et al., 2008). Theoretically, lakes with wind and hydrological forces in the same direction may advect biomass along the shoreline beyond the detection of the satellite (Chorus et al., 2000; Rogalus and Watzin, 2008). The spatial resolution of MERIS and OLCI along with flags that mask the land-water interface limit measures along these shorelines. Lakes with wind and hydrologic forces in opposing directions, or lower energy, may have biomass toward the center of the system or biomass may vertically mixed. As we are using satellite sensors that detect in the near-infrared and red wavelengths of the electromagnetic spectrum, whole lake cell density can be underestimated when a bloom is distributed throughout the water column, or biomass may be missed if completely below the satellites depth of detection.

The near-infrared and red wavelengths often used in cyanobacteria detection attenuate rapidly with depth and therefore do not penetrate as deep into the water column compared to green and blue wavelengths (Kirk, 1994). CI_{cyano} characterizes the upper layer of the water column, including depths up to 2 m in clear water (Mishra et al., 2005) and less than 2 m in more turbid water (Wynne et al., 2010). The CI_{cyano} algorithm has uncertainty where validations demonstrated 84% overall agreement against state reported toxin data (Mishra et al., 2021), 73% overall agreement against state reported events and advisories (Whitman et al., In Press), and 60% mean absolute error with 11% bias against chlorophyll-a at the national scale (Seegers et al., 2021).

Recent OLCI calibration efforts have revealed a 1-1.5% brightness bias between Sentinel-3A and -3B, but the spectral consistency in this bias should not affect the CI_{cyano} calculation (OLCI ESL, 2019). Wynne et al. (2021) recently reported a method to intercalibrate MERIS and OLCI to MODIS across the Great Lakes, where OLCI CI_{cyano} underestimated MERIS CI_{cyano} by 6%. However, MODIS would not be able to fill the temporal gaps for most of the resolved lakes in this study due to its pixel size limitations (1-km spatial resolution). The OLCI CI_{cyano} underestimation relative to MERIS was not necessarily an issue in this study because all the CI_{cyano} derived values were categorized as detections. The quantification of a minimum detection limit for both the OLCI and MERIS sensors was relevant to this study to determine if CI_{cyano} was detecting cyanobacteria biomass at the same minimum level between the two time periods. MERIS and OLCI are two different sensors during two different time periods, and therefore the measured temporal change was constrained to each respective time period without interpretation of change during the gap years. Satellite sensor radiometric instrument drift was also a potential limitation, where current OLCI radiometric gain model performance were reported within 0.1% root mean square (Bourg et al., 2021).

The findings of this study and the approaches used to provide them pave the way for future inland cyanoHAB assessments. These results build upon the findings from numerous studies (Andersen et al., 2017; De Bakker et al., 2017; Svirčev et al., 2017; Xu et al., 2017; Ho et al., 2019) on inland waters by using satellite data to extend temporal assessment for cyanobacteria blooms to a national and state scale and across numerous waterbodies. On a broader scale, the temporal assessment method demonstrated here can be applied to other satellite sensors, different cyanobacteria detection algorithms, and to other lakes in countries experiencing inland cyanobacteria dominance. This work provides an opportunity for each state to have a uniform satellite dataset (Schaeffer et al., 2015) and a consistent approach for determining the spatial extent and rate of change of cyanoHABs, year-to-year, with long-term operational satellites. Further, this study reinforces the value that satellite remote sensing can add to *in situ* water quality monitoring programs to quantitatively evaluate change.

The analysis of drivers was beyond the scope of one paper but has been reported through other analyses using the same satellite data time series (Myer et al., 2020; Iiames et al., 2021). Briefly, Iiames et al (2021) reported variable importance for 75 landscape and lake physiographic predictor variables including nutrients, artificial drainage, buffer space, precipitation, and temperature. The top ten predictor variables were artificial drainage, percent area forest, soil erodibility, subsurface nitrogen-ammonia application rate, percent evergreen forest, percent area row crop, surface nitrate application rate, runoff, percent area evergreen forest within a 90m lake buffer, and percent sinks that treat agriculture (Iiames et al., 2021). Myer et al (2020) reported surface water temperature, ambient temperature, precipitation, and lake geomorphology as important covariates. Wilkinson et al. (2021) reported a similar lack of intensification across 323 lakes (Soranno et al., 2015) in the upper Midwest and northeastern United States between 2000 and 2012, supporting the mixed

spatial extent responses during the 2008–2011 time series presented in this study and highlighting the importance of acknowledging the temporal limitations in these assessments. Integration of local-scale models may further elucidate causative changes in the water and sediment quality of lake environments such as nutrient enrichment and minerology that may either initiate or sustain cyanoHAB events (Santhanam et al., 2018). Further analysis may also benefit from local scale assessments of built infrastructure such as impervious surfaces and urbanization rates (Santhanam and Majumdar, 2022). Hence the spatial extent of these events may vary depending on the degree of nutrient cycling and landscape influence, however, access to real time nutrient data at the same scale as the satellite data is currently a limiting observation.

5 Conclusions

We used an assessment method combined with satellite remote sensing data to quantify the spatial extent of cyanobacterial blooms across the contiguous United States. Cyanobacteria spatial extent varied seasonally, reaching maximum spatial extent during late summer into autumn (August-October). There was a strong national and moderate South and Southeast region increase in cyanoHAB spatial extent during 2017–2020, but there was no ubiquitous increase or decrease in cyanoHAB spatial extent during 2008–2011 at the national or region scales. There were 12 states with strong or moderate increases during 2017–2020, while only one state had a moderate increase in spatial extent during 2008–2011 and two states with a moderate decrease. CyanoHAB spatial extent changes varied dependent on spatial and temporal scales considered. A decline, or no change, in cyanoHAB surface area extent does not indicate a lack of issues related to cyanoHABs. This study is the first to quantify the spatial extent of cyanoHABs for lakes across CONUS with a standard assessment method to report rates of change as a consistent indicator metric. These findings can be used to help prioritize events and quantify if cyanoHABs are increasing, decreasing, or remain unchanged. As previously reported these satellite metrics may help inform recreational, drinking, and water quality management in metropolitan and rural areas across federal, state, and tribal lands (Papenfus et al., 2020; Stroming et al., 2020; Coffer et al., 2021b). This may result in better environmental, human, and animal health protection.

Acknowledgments: E.U., M.C., B.S. conducted the research, conducted data preprocessing, and analyzed the data. B.S., K.L., R.S., P.J.W., M.C., and W.S. contributed to the interpretation and discussion of the results. All authors substantially participated in the writing of the manuscript. E.U. and B.S. conceived of the research. P.J.W. and R.S. provided MERIS datasets and CI_{cyano} products. This article has been reviewed by the Center for Environmental Measurement and approved for publication. Mention of trade names or commercial products does not constitute endorsement or recommendation for use by the US Government. The views expressed in this article are those of the authors and do not necessarily reflect the views or policies of the US EPA. Authors declare no competing interests. All data and code will be made available at the following DOI after acceptance: https://doi.org/TBD.

Funding Sources: This material is based upon work supported by the NASA Ocean Biology and Biogeochemistry Program/Applied Sciences Program (proposals 14-SMDUNSOL14- 0001 and SMDSS20-0006) and by the US EPA, NOAA, US Geological Survey Toxic Substances Hydrology Program, and Oak Ridge Institute for Science and Technology. Additional resources

were provided through an EPA Environmental Modeling and Visualization Laboratory (EMVL) and High-Performance Computing (HPC) award.

Table 1. Seasonal Mann-Kendall statistics for changes in monthly cyanobacteria spatial extent spanning 2017–2020 for each CONUS region as defined by Karl and Koss (1984). Bold values represent moderate ($0.3 \leq |\tau| < 0.5$) through strong ($|\tau| \geq 0.5$) Kendall τ strength. Change in spatial extent over time period is generated from the seasonal Kendall slope estimator and represents the change in spatial extent (%) over the entire time period spanning 2017–2020. The γ statistic is an estimate of the number of years of observations required for the observed change to outweigh variability in the data. See Supplemental Table S2 for years 2008–2011.

Region	Sample size	Change in spatial extent over time period	Kendall's τ	γ (yr)
Northeast	48	10.8%	0.22	4.51
Northwest	48	2.84%	0.19	14.96
Northwest Rockies and Plains	48	1.89%	0.19	15.03
Ohio Valley	48	0.1%	0.01	> 100
South	**48**	**8.58%**	**0.36**	**3.55**
Southeast	**48**	**10.93%**	**0.31**	**3.91**
Southwest	48	1.76%	0.22	14.6
Upper Midwest	47	5.08%	0.15	17.22
West	48	3.88%	0.28	8.13

Table 2. Seasonal Mann-Kendall statistics for changes in monthly cyanobacteria spatial extent spanning 2017–2020 for each CONUS state with at least one resolvable lake (see Fig. 3). Bold values represent moderate ($0.3 \leq |\tau| < 0.5$) through strong ($|\tau| \geq 0.5$) seasonal Kendall τ strength. Change in spatial extent over time period represents the change in spatial extent (%) over the entire time period spanning 2017–2020. The γ statistic is an estimate of the number of years of observations required for the observed change to outweigh variability in the data. See Supplemental Table S1 for years 2008–2011.

State name	State abbreviation	Sample size	Change in spatial extent over time period	Kendall's τ	γ (yr)
Alabama	AL	48	2.32%	0.18	7.02
Arizona	**AZ**	**48**	**8.09%**	**0.36**	**4.38**
Arkansas	AR	48	-6.59%	0.22	6.45
California	CA	48	1.96%	0.19	19.4
Colorado	CO	47	14.02%	0.24	3.9
Connecticut	CT	47	0%	0.05	*N/A**
Florida	**FL**	**48**	**15.06%**	**0.31**	**4.45**
Georgia	GA	48	3.72%	0.19	5.32
Idaho	ID	46	3.23%	0.26	15.04
Illinois	IL	48	6.52%	0.11	14.18
Indiana	IN	48	-2.67%	0.06	23.13
Iowa	IA	45	-10.24%	0.13	10.75
Kansas	KS	48	3.91%	0.08	20.39
Kentucky	KY	48	0.46%	0.13	53.31
Louisiana	**LA**	**48**	**17.8%**	**0.53**	**2.84**
Maine	**ME**	**42**	**10.73%**	**0.3**	**7.72**
Maryland	MD	48	0%	0.15	*N/A**
Massachusetts	**MA**	**48**	**42.38%**	**0.39**	**2.33**
Michigan	**MI**	**47**	**10.5%**	**0.38**	**3.68**
Minnesota	MN	40	3.52%	0.11	24.17
Mississippi	MS	48	-6.16%	0.14	14.65
Missouri	MO	48	11.84%	0.17	3.83
Montana	**MT**	**45**	**3.98%**	**0.37**	**5.31**
Nebraska	NE	46	0.98%	0.02	55.88
Nevada	NV	48	11.8%	0.28	5
New Hampshire	**NH**	**39**	**14.22%**	**0.33**	**5.41**
New Jersey	**NJ**	**48**	**24.75%**	**0.51**	**3.14**
New Mexico	NM	48	5.87%	0.24	7.17
New York	NY	48	3.07%	0.17	13.88

North Carolina	NC	48	3.2%	0.22	14.14
North Dakota	ND	38	-1.7%	0.17	18.29
Ohio	OH	46	-6.17%	0.15	13.98
Oklahoma	OK	48	2.68%	0.1	14.41
Oregon	**OR**	**48**	**8.09%**	**0.42**	**8.07**
Pennsylvania	PA	47	-4.63%	0.12	15.72
Rhode Island	RI	48	16.63%	0.29	5.83
South Carolina	SC	48	0.29%	0.07	44.06
South Dakota	**SD**	**41**	**4.01%**	**0.48**	**6.38**
Tennessee	TN	48	-2.54%	0.18	8.11
Texas	TX	48	-0.49%	0.03	83.6
Utah	UT	48	1.3%	0.14	21.89
Vermont	**VT**	**46**	**4.6%**	**0.38**	**5.4**
Virginia	VA	48	0.49%	0.06	73.84
Washington	WA	48	4.89%	0.17	8.11
Wisconsin	WI	43	0%	0	*N/A**
Wyoming	WY	43	3.26%	0.2	12.37
CONUS		**48**	**6.92**	**0.56**	**2.87**

* The γ statistic requires the change in spatial extent over the time period as the denominator; thus, with a change of 0%, γ was not computed.

712 **Table 3.** Seasonal Kendall's τ values highlighting strength of change in monthly cyanobacteria
713 spatial extent spanning 2017–2020 for each CONUS state with at least one resolvable lake at
714 10%, 20%, and 30% random weekly composite omission. Bold values represent moderate ($0.3 \leq$
715 $|\tau| < 0.5$) through strong ($|\tau| \geq 0.5$) seasonal Kendall τ strength.

State name	State abbreviation	τ (from Table 2)	τ (10% data omission)	τ (20% data omission)	τ (30% data omission)
AL	Alabama	0.18	0.19	0.21	**0.42**
AR	Arkansas	0.22	-0.19	-0.12	-0.23
AZ	Arizona	**0.36**	**0.36**	**0.36**	**0.33**
CA	California	0.19	0.19	0.25	0.23
CO	Colorado	0.24	0.24	0.26	**0.33**
CT	Connecticut	0.05	-0.04	-0.08	0.08
FL	Florida	**0.31**	**0.33**	**0.39**	**0.3**
GA	Georgia	0.19	0.11	0.17	0.1
IA	Iowa	0.13	-0.2	-0.15	-0.27
ID	Idaho	0.26	0.22	**0.3**	0.29
IL	Illinois	0.11	0.06	0.03	0.1
IN	Indiana	0.06	-0.07	-0.09	-0.1
KS	Kansas	0.08	0.08	0.09	0.07
KY	Kentucky	0.13	0.06	0.09	0.18
LA	Louisiana	**0.53**	**0.5**	**0.44**	**0.42**
MA	Massachusetts	**0.39**	**0.36**	**0.56**	**0.33**
MD	Maryland	0.15	0.14	0.15	0.06
ME	Maine	**0.3**	0.26	**0.3**	0.25
MI	Michigan	**0.38**	**0.41**	**0.35**	0.15
MN	Minnesota	0.11	0.25	0.13	0
MO	Missouri	0.17	0.11	0.19	0.23
MS	Mississippi	0.14	-0.14	-0.14	-0.14
MT	Montana	**0.37**	**0.38**	**0.38**	**0.33**
NC	North Carolina	0.22	0.19	0.22	0.22
ND	North Dakota	0.17	-0.13	**-0.38**	-0.2
NE	Nebraska	0.02	-0.03	-0.04	-0.11
NH	New Hampshire	**0.33**	0.29	**0.38**	**0.39**
NJ	New Jersey	**0.51**	**0.48**	**0.48**	**0.56**
NM	New Mexico	0.24	0.25	0.25	**0.33**
NV	Nevada	0.28	0.28	0.28	**0.52**
NY	New York	0.17	0.14	0.03	0.07
OH	Ohio	0.15	-0.2	**-0.33**	**-0.3**
OK	Oklahoma	0.1	0.11	0.08	-0.06
OR	Oregon	0.42	0.42	0.5	0.56

PA	Pennsylvania	0.12	-0.1	-0.15	-0.19
RI	Rhode Island	0.29	**0.33**	**0.39**	**0.33**
SC	South Carolina	0.07	-0.03	0	-0.1
SD	South Dakota	**0.48**	**0.43**	**0.33**	**0.42**
TN	Tennessee	0.18	-0.28	-0.19	**-0.3**
TX	Texas	0.03	-0.11	0.03	-0.03
UT	Utah	0.14	0.21	0.13	0.07
VA	Virginia	0.06	0.07	0.08	-0.01
VT	Vermont	**0.38**	**0.44**	**0.48**	**0.42**
WA	Washington	0.17	0.25	0.15	0.1
WI	Wisconsin	0	-0.1	-0.11	0
WY	Wyoming	0.2	0.22	0.11	0.1
CONUS		**0.56**	**0.47**	**0.44**	**0.44**

716
717
718

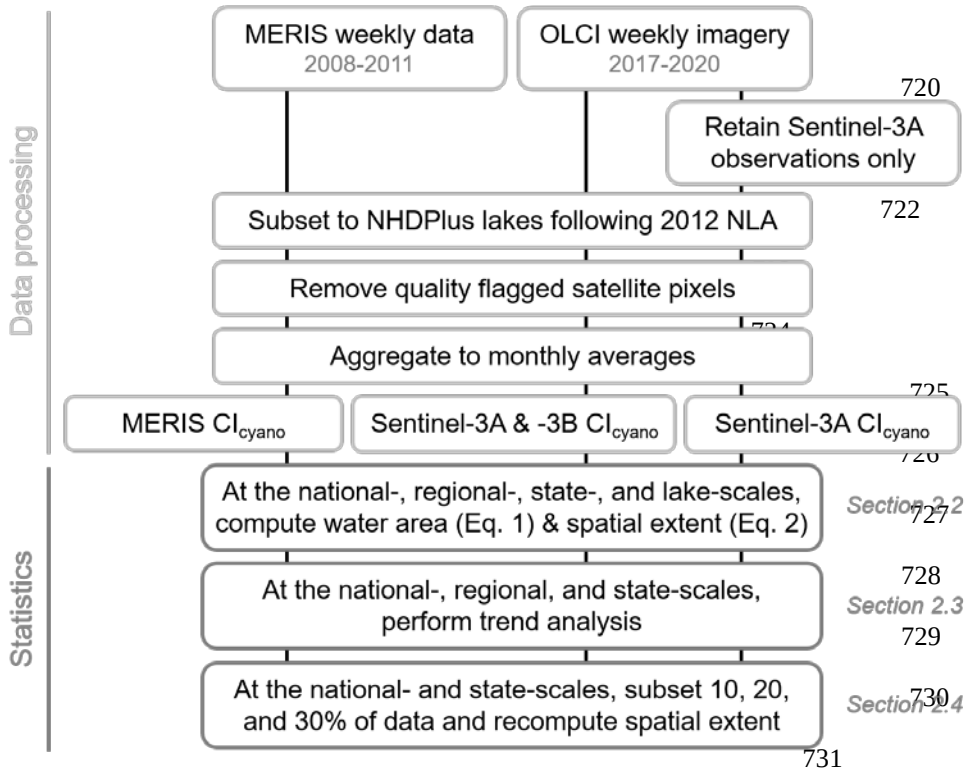

Fig. 1. A representation of the approach used for data processing and statistics described in detail from Sections 2.1 through 2.4.

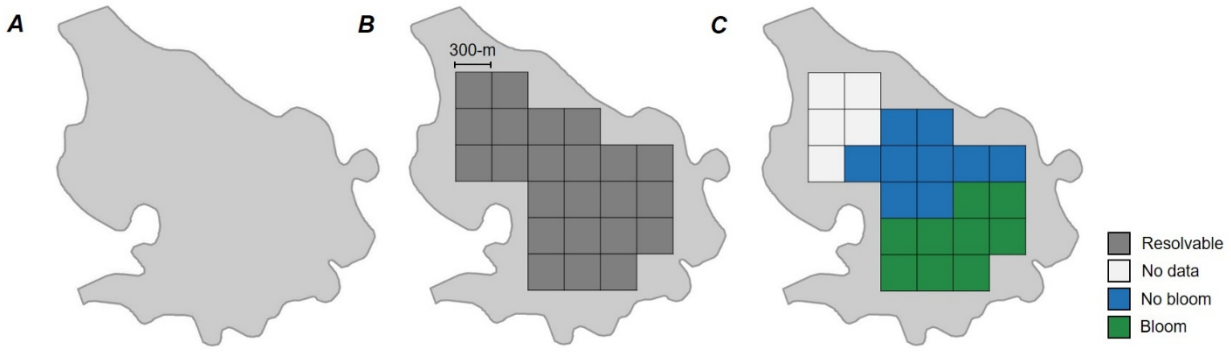

Fig 2. A conceptual diagram illustrating the computation of resolvable water area and cyanobacterial spatial extent. For each (A) resolvable lake, (B) resolvable water area was computed as the number of 300-m satellite pixels within the lake, and (C) spatial extent was computed as the number of pixels with detectable cyanobacteria ("bloom") divided by the number of valid pixels (sum of "No bloom" and "Bloom").

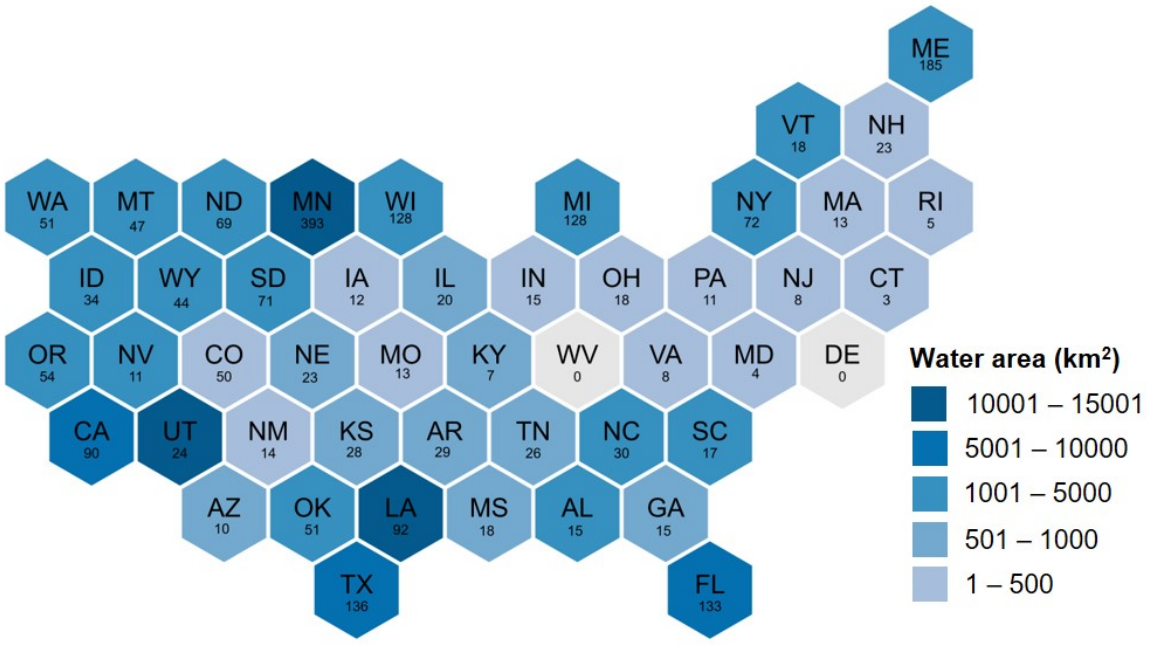

Fig 3. Median satellite resolvable water area (km^2) for 2017–2020 for each state at a spatial resolution of 300 m. Each state is represented as a hexagon labeled with two-letter state abbreviation. WV and DE are presented in gray as they have no satellite resolvable water at a spatial resolution of 300 m. Below each two-letter state abbreviation is the number of individual state NHDPlus lakes. Lakes that fell along the boundary of more than one state were counted for each state they intercepted; therefore, the total number of lakes shown in this figure totals 2,270, more than the 2,192 lakes resolvable with 300-m MERIS and OLCI imagery.

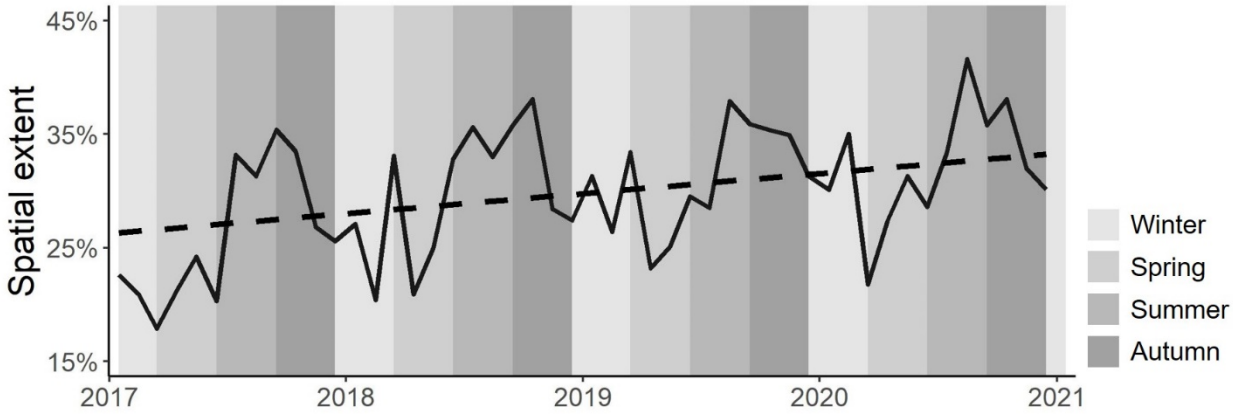

Fig. 4. Monthly spatial extent (%) of any detectable cyanoHAB for CONUS for 2017–2020. Shaded plot regions delineate meteorological seasons. The dashed line represents the seasonal Kendall slope estimator accompanying a seasonal Mann-Kendall test applied to monthly observations. See Supplemental Fig. S3 for years 2008–2011.

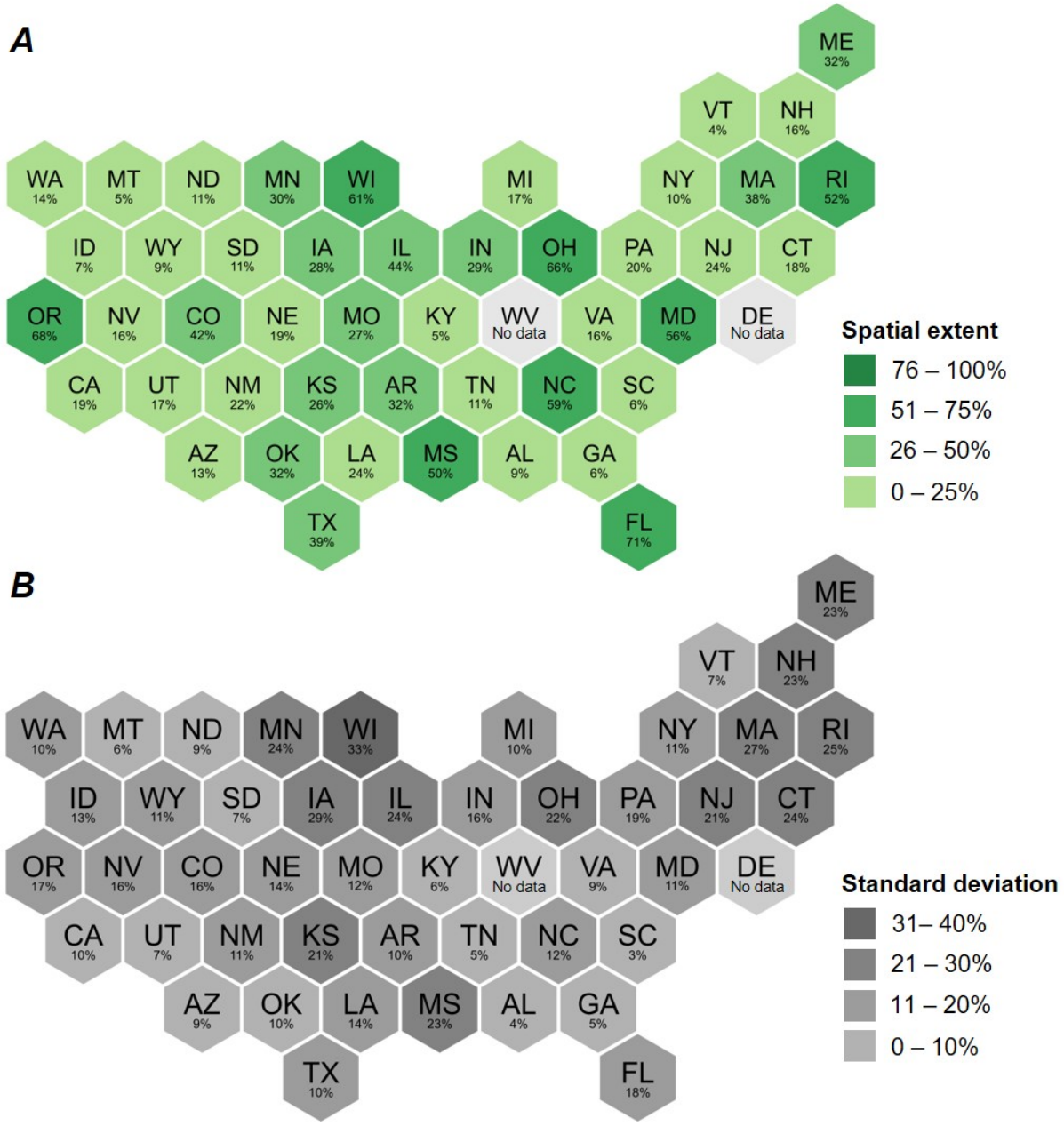

Fig. 5. (A) Median and (B) standard deviation spatial extent for each CONUS state for 2017–2020. Each state is represented as a hexagon labeled with each state's two-letter state abbreviation. WV and DE are presented in light gray as they have no satellite resolvable water at a spatial resolution of 300 m. See Supplemental Fig. 4 for years 2008–2011.

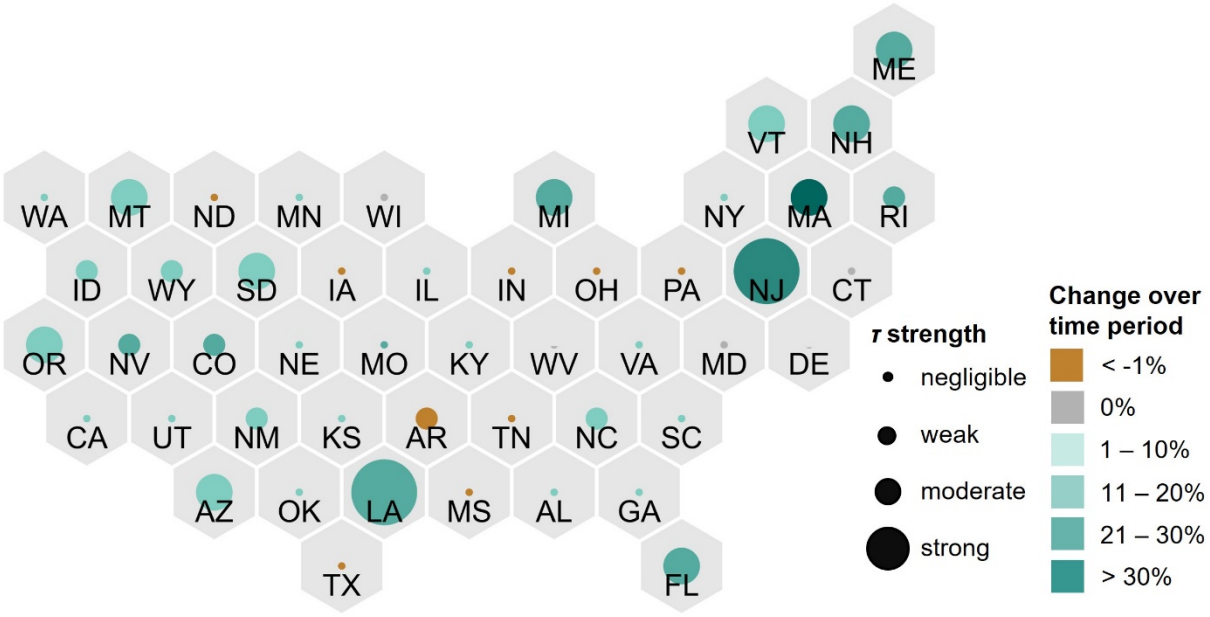

Fig. 6. Change in spatial extent in each CONUS state for 2017–2020 based on results from the seasonal Mann-Kendall test. Each state is represented as a hexagon labeled with each state's two-letter state abbreviation. WV and DE have no results as they have no satellite resolvable water at a spatial resolution of 300 m. Color of circles illustrates change over time period, where brown indicates a decrease in bloom area during 2017–2020 and shades of green indicate an increase; size of circles represent categorical Kendall τ, where $|\tau| < 0.2$ denotes a negligible change, $0.2 \leq |\tau| < 0.3$ denotes a weak change, $0.3 \leq |\tau| < 0.5$ denotes a moderate change and $|\tau| \geq 0.5$ denotes a strong change. See Supplemental Fig. S5 for years 2008–2011.

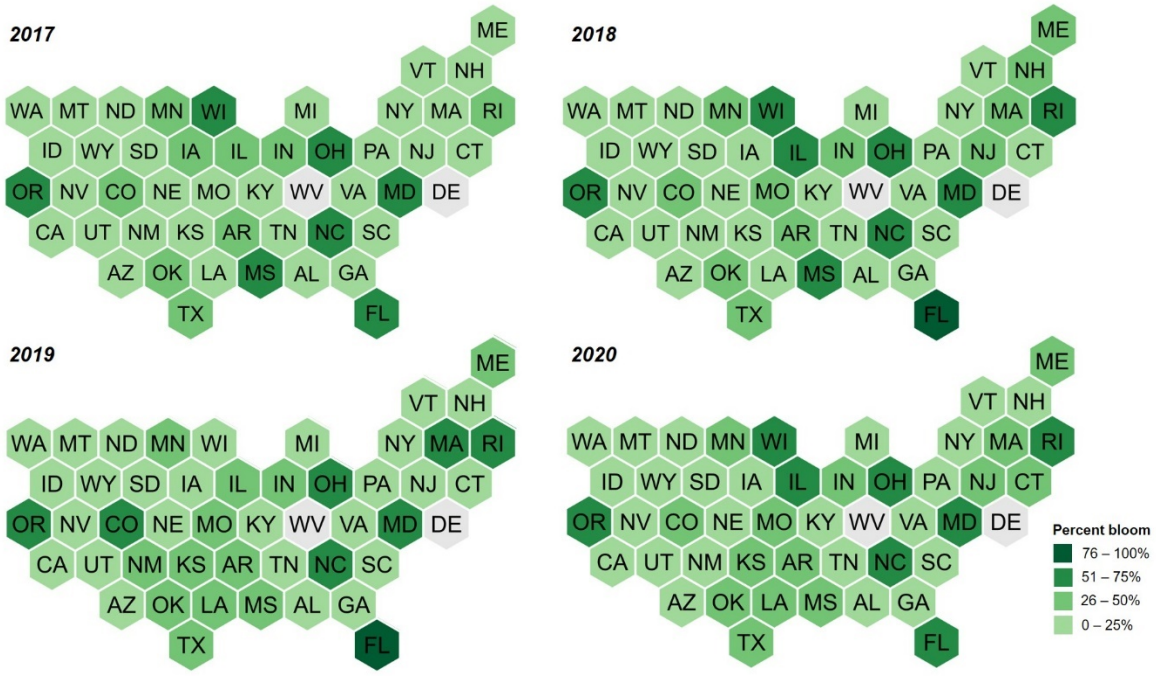

Fig. 7. Spatial extent for each CONUS state for 2017–2020. Each state is represented as a hexagon labeled with each state's two-letter state abbreviation. WV and DE are presented in gray as they have no satellite resolvable water at a spatial resolution of 300 m. See Supplemental Fig. S6 for years 2008–2011.

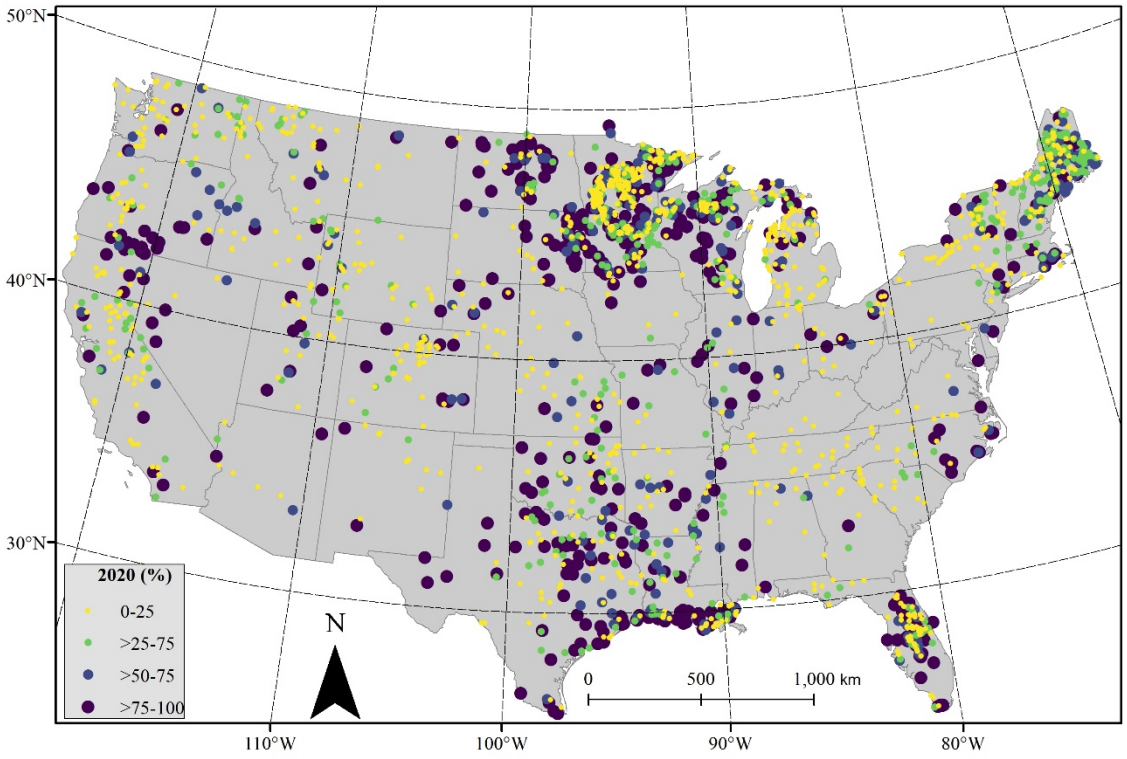

Fig. 8. Median annual spatial extent for each resolvable lake for the year 2020. Each point represents a lake centroid. See Supplemental Fig. S7-S9 for years 2017–2020 and Supplemental Fig. S10-S13 for years 2008–2011.

References

Akoglu, H., 2018. User's guide to correlation coefficients. Turk J Emerg Med 18, 91-93.

Andersen, J.H., Carstensen, J., Conley, D.J., Dromph, K., Fleming-Lehtinen, V., Gustafsson, B.G., Josefson, A.B., Norkko, A., Villnäs, A., Murray, C., 2017. Long-term temporal and spatial trends in eutrophication status of the Baltic Sea. Biological Reviews 92, 135-149.

Anderson, D.M., 1989. Toxic algal blooms and red tides: a global perspective., in: Okaichi, D., Anderson, M., Nemoto, T. (Eds.), Redtides: biology, environmental science, and toxicology. Elsevier, New York, New York, USA, pp. 11-16.

Anderson, D.M., Glibert, P.M., Burkholder, J.M., 2002. Harmful algal blooms and eutrophication: Nutrient sources, composition, and consequences. Estuaries 25, 704-726.

Bourg, L., Smith, D., Rouffi, F., Hénocq, C., Bruniquel, J., Cox, C., Etxaluze, M., Polehampton, E., 2021. S3MPC OPT Annual Performance Report - Year 2020. Preparation and operations of the mission performance center for the Copernicus Sentinel-3 mission. S3MPC.ACR.APR.007.

Chen, Y., Qin, B., Teubner, K., Dokulil, M.T., 2003. Long-term dynamics of phytoplankton assemblages: *Microcystis*-domination in Lake Taihu, a large shallow lake in China. Journal of Plankton Research 25, 445-453.

Cheruvelil, K.S., Soranno, P.A., McCullough, I.M., Webster, K.E., Rodriguez, L.K., Smith, N.J., 2021. LAGOS-US LOCUSv1.0: Data module of location, identifiers, and physical characteristics of lakes and their watersheds in the conterminous U.S. Limnology and Oceanography Letters 6, 270-292.

Chorus, E.I., Bartram, J., 1999. Toxic cyanobacteria in water: a guide to their public health consequences, monitoring and management.

Clark, J.M., Schaeffer, B.A., Darling, J.A., Urquhart, E.A., Johnston, J.M., Ignatius, A.R., Myer, M.H., Loftin, K.A., Werdell, P.J., Stumpf, R.P., 2017. Satellite monitoring of cyanobacterial harmful algal bloom frequency in recreational waters and drinking water sources. Ecological Indicators 80, 84-95.

Coffer, M., Schaeffer, B., Darling, J., Urquhart, E., Salls, W., 2020. Quantifying national and regional cyanobacterial occurrence in US lakes using satellite remote sensing. Ecological Indicators 111, https://doi.org/10.1016/j.ecolind.2019.105976.

Coffer, M., Schaeffer, B., Salls, W., Urquhart, E., Loftin, K., Stumpf, R., Werdell, P., Darling, J., 2021a. Satellite remote sensing to assess cyanobacterial bloom frequency across the United States at multiple spatial scales. Ecological Indicators 128, 107822.

Coffer, M.M., Hestir, E.L., 2019. Variability in Trends and Indicators of CO

2

Exchange Across Arctic Wetlands. Journal of Geophysical Research: Biogeosciences 124, 1248-1264.

Coffer, M.M., Schaeffer, B.A., Foreman, K., Porteous, A., Loftin, K.A., Stumpf, R.P., Werdell, P.J., Urquhart, E., Albert, R.J., Darling, J.A., 2021b. Assessing cyanobacterial frequency and abundance at surface waters near drinking water intakes across the United States. Water Research 201, 117377.

Cohen, J., 1988. Differences between correlation coefficients., in: Cohen, J. (Ed.), Statistical power analysis for the behavioral sciences., 2nd ed. Lawrence Erlbaum Associates Publishers, Hillsdale, pp. 109-143.

Cuypers, Y., Vincon-Leite, B., Groleau, A., Tassin, B., Humbert, J.F., 2011. Impact of internal waves on the spatial distribution of Planktothrix rubescens (cyanobacteria) in an alpine lake. ISME J 5, 580-589.

De Bakker, D.M., Van Duyl, F.C., Bak, R.P., Nugues, M.M., Nieuwland, G., Meesters, E.H., 2017. 40 Years of benthic community change on the Caribbean reefs of Curaçao and Bonaire: the rise of slimy cyanobacterial mats. Coral Reefs 36, 355-367.

Deng, J., Qin, B., Paerl, H.W., Zhang, Y., Ma, J., Chen, Y., 2014. Earlier and warmer springs increase cyanobacterial (Microcystis spp.) blooms in subtropical Lake Taihu, China. Freshwater Biology 59, 1076-1085.

Duan, H., Ma, R., Xu, X., Kong, F., Zhang, S., Kong, W., Hao, J., Shang, L., 2009. Two-decade reconstruction of algal blooms in China's Lake Taihu. Environmental Science & Technology 43, 3522-3528.

Elliott, J.A., 2010. The seasonal sensitivity of Cyanobacteria and other phytoplankton to changes in flushing rate and water temperature. Global Change Biology 16, 864-876.

Glass, G.V., 1966. Note on Rank Biserial Correlation. Educational and Psychological Measurement 26, 623-631.

Gleason, K.L., Lawrimore, J.H., Levinson, D.H., Karl, T.R., Karoly, D.J., 2008. A Revised U.S. Climate Extremes Index. Journal of Climate 21, 2124-2137.

Gómez, J.A.D., Alonso, C.A., García, A.A., 2011. Remote sensing as a tool for monitoring water quality parameters for Mediterranean Lakes of European Union water framework directive (WFD)

and as a system of surveillance of cyanobacterial harmful algae blooms (SCyanoHABs). Environmental Monitoring and Assessment 181, 317-334.

Gonzalez-Piana, M., Piccardo, A., Ferrer, C., Brena, B., Pirez, M., Fabian, D., Chalar, G., 2018. Effects of Wind Mixing in a Stratified Water Column on Toxic Cyanobacteria and Microcystin-LR Distribution in a Subtropical Reservoir. Bull Environ Contam Toxicol 101, 611-616.

Hallegraeff, G.M., 1993. A review of harmful algal blooms and their apparent global increase. Phycologia 32, 79-99.

Hallegraeff, G.M., Anderson, D.M., Belin, C., Bottein, M.Y.D., Bresnan, E., Chinain, M., Enevoldsen, H., Iwataki, M., Karlson, B., McKenzie, C.H., Sunesen, I., Pitcher, G.C., Provoost, P., Richardson, A., Schweibold, L., Tester, P.A., Trainer, V.L., Yñiguez, A.T., Zingone, A., 2021. Perceived global increase in algal blooms is attributable to intensified monitoring and emerging bloom impacts. Communications Earth and Environment 2, 117.

Helsel, D.R., Hirsch, R.M., Ryberg, K.R., Archfield, S.A., Gilroy, E.J., 2020. Statistical methods in water resources.

Henson, S.A., Sarmiento, J.L., Dunne, J.P., Bopp, L., Lima, I., Doney, S.C., John, J., Beaulieu, C., 2010. Detection of anthropogenic climate change in satellite records of ocean chlorophyll and productivity. Biogeosciences 7, 621-640.

Hirsch, R.M., Slack, J.R., 1984. A nonparametric trend test for seasonal data with serial dependence. Water Resources Research 20, 727-732.

Hirsch, R.M., Slack, J.R., Smith, R.A., 1982. Techniques of trend analysis for monthly water quality data. Water Resources Research 18, 107-121.

Ho, J.C., Michalak, A.M., 2019. Exploring temperature and precipitation impacts on harmful algal blooms across continental U.S. lakes. Limnology and Oceanography 65, 992-1009.

Ho, J.C., Michalak, A.M., Pahlevan, N., 2019. Widespread global increase in intense lakea phytoplankton blooms since the 1980s. Nature 574, 667-670.

Iiames, J.S., Salls, W., Mehaffey, M.H., Nash, M.S., Christensen, J., Schaeffer, B., 2021. Modelling anthropogenic and environmental influences on freshwater harmful algal bloom development detected by MERIS over the Central United States. Water Resources Research.

Jancula, D., Marsalek, B., 2011. Critical review of actually available chemical compounds for prevention and management of cyanobacterial blooms. Chemosphere 85, 1415-1422.

Jin, Q., Lyu, H., Shi, L., Miao, S., Wu, Z., Li, Y., Wang, Q., 2017. Developing a two-step method for retrieving cyanobacteria abundance from inland eutrophic lakes using MERIS data. Ecological Indicators 81, 543-554.

Kahru, M., Elmgren, R., 2014. Multidecadal time series of satellite-detected accumulations of cyanobacteria in the Baltic Sea. Biogeosciences 11, 3619-3633.

Kahru, M., Elmgren, R., Savchuk, O.P., 2016. Changing seasonality of the Baltic Sea. Biogeosciences 13, 1009-1018.

Kahru, M., Kudela, R.M., Manzano-Sarabia, M., Greg Mitchell, B., 2012. Trends in the surface chlorophyll of the California Current: Merging data from multiple ocean color satellites. Deep Sea Research Part II: Topical Studies in Oceanography 77-80, 89-98.

Karl, T., Koss, W.J., 1984. Regional and national monthly, seasonal, and annual temperature weighted by area, 1895-1983.

Kendall, M.G., 1938. A new measure of rank correlation. Biometrika 30, 81-93.

Kim, S.W., Heckel, A., Frost, G.J., Richter, A., Gleason, J., Burrows, J.P., McKeen, S., Hsie, E.Y., Granier, C., Trainer, M., 2009. NO2columns in the western United States observed from space and simulated by a regional chemistry model and their implications for NOxemissions. Journal of Geophysical Research 114.

Kirk, J.T.O., 1994. Light and Photosynthesis in Aquatic Ecosystems. Cambridge University Press, New York.

Komatsu, E., Fukushima, T., Harasawa, H., 2007. A modeling approach to forecast the effect of long-term climate change on lake water quality. Ecological Modelling 209, 351-366.

Kutser, T., Metsamaa, L., Dekker, A.G., 2008. Influence of the vertical distribution of cyanobacteria in the water column on the remote sensing signal. Estuarine, Coastal and Shelf Science 78, 649-654.

Kutser, T., Metsamaa, L., Strömbeck, N., Vahtmäe, E., 2006. Monitoring cyanobacterial blooms by satellite remote sensing. Estuarine, Coastal and Shelf Science 67, 303-312.

Li, Y., He, R., 2014. Spatial and temporal variability of SST and ocean color in the Gulf of Maine based on cloud-free SST and chlorophyll reconstructions in 2003–2012. Remote sensing of environment 144, 98-108.

Lin, Q., Zhang, K., McGowan, S., Capo, E., Shen, J., 2021. Synergistic impacts of nutrient enrichment and climate change on long-term water quality and ecological dynamics in contrasting shallow-lake zones. Limnology and Oceanography 66, 3271-3286.

Loftin, K.A., Graham, J.L., Hilborn, E.D., Lehmann, S.C., Meyer, M.T., Dietze, J.E., Griffith, C.B., 2016. Cyanotoxins in inland lakes of the United States: Occurrence and potential recreational health risks in the EPA National Lakes Assessment 2007. Harmful Algae 56, 77-90.

Lunetta, R., Schaeffer, B.A., Keith, D.J., Jacobs, S., Stumpf, R.P., Murphy, M., 2015. Evaluation of cyanobacteria cell count detection derived from MERIS imagery across the eastern USA. Remote Sensing of Environment 157.

Mann, H.B., 1945. Nonparametric tests against trend. Econometrica: Journal of the Econometric Society, 245-259.

Mann, H.B., Whitney, D.R., 1947. On a Test of Whether one of Two Random Variables is Stochastically Larger than the Other. The Annals of Mathematical Statistics 18, 50-60.

Marchetto, A., 2017. rkt: Mann-Kendall Test, Seasonal and Regional Kendall Tests.

Matthews, M.W., 2014. Eutrophication and cyanobacterial blooms in South African inland waters: 10 years of MERIS observations. Remote Sensing of Environment 155, 161-177.

Matthews, M.W., Bernard, S., Robertson, L., 2012. An algorithm for detecting trophic status (chlorophyll-a), cyanobacterial-dominance, surface scums and floating vegetation in inland and coastal waters. Remote Sensing of Environment 124, 637-652.

Matthews, M.W., Odermatt, D., 2015. Improved algorithm for routine monitoring of cyanobacteria and eutrophication in inland and near-coastal waters. Remote Sensing of Environment 156, 374-382.

McKay, L., Bondelid, T., Dewald, T., Johnston, J., Moore, R., Rea, A., 2012. NHDPlus Version 2: User Guide. US Environmental Protection Agency.

Mélin, F., 2016. Impact of inter-mission differences and drifts on chlorophyll-atrend estimates. International Journal of Remote Sensing 37, 2233-2251.

Melin, F., Vantrepotte, V., Chuprin, A., Grant, M., Jackson, T., Sathyendranath, S., 2017. Assessing the fitness-for-purpose of satellite multi-mission ocean color climate data records: A protocol applied to OC-CCI chlorophyll-a data. Remote Sensing of Environment 203, 139-151.

Michalak, A.M., Anderson, E.J., Beletsky, D., Boland, S., Bosch, N.S., Bridgeman, T.B., Chaffin, J.D., Cho, K., Confesor, R., Daloğlu, I., 2013. Record-setting algal bloom in Lake Erie caused by

agricultural and meteorological trends consistent with expected future conditions. Proceedings of the National Academy of Sciences 110, 6448-6452.

Mishra, D.R., Narumalani, S., Rundquist, D.C., Lawson, M., 2005. Characterizing the vertical diffuse attenuation coefficient for downwelling irradiance in coastal waters: Implications for water penetration by high resolution satellite data. Journal of Photogrammetry and Remote Sensing 60, 48-64.

Mishra, S., R.P.Stumpf, Schaeffer, B., Werdell, P.J., Loftin, K.A., Meredith, A., 2021. Evaluation of a satellite-based cyanobacteria bloom detection algorithm using field-measured Microcystin data. Science of the Total Environment, 145462.

Mishra, S., Stumpf, R., Schaeffer, B., Werdell, P., Loftin, K., Meredith, A., 2019. Measurement of cyanobacterial bloom magnitude using satellite remote sensing. Scientific Reports 9, 1-17.

Moradi, M., 2014. Comparison of the efficacy of MODIS and MERIS data for detecting cyanobacterial blooms in the southern Caspian Sea. Marine Pollution Bulletin 87, 311-322.

Myer, M.H., Urquhart, E., Schaeffer, B.A., Johnston, J.M., 2020. Spatio-temporal modeling for forecasting high-risk freshwater cyanobacterial harmful algal blooms in Florida. Frontiers in Environmental Science 8, 581091.

NOAA, 2021. Historical El Nino / La Nina episodes (1950s-present). National Weather Service Climate Prediction Center, http://www.cpc.noaa.gov/products/analysis_monitoring/ensostuff/ensoyears.shtml.

OLCI ESL, 2019. Sentinel-3 OLCI Cyclic Performance Report. Mission Performance Centre S3MPC.ACR.PR.01-040-021.

Omernik, J.M., 1995. Ecoregions: A spatial framework for environmental management. Lewis Publishers, Boca Raton, FL.

Omernik, J.M., Griffith, G.E., 2014. Ecoregions of the conterminous United States: evolution of a hierarchical spatial framework. Environmental Management 54, 1249-1266.

Paerl, H.W., Hall, N.S., Calandrino, E.S., 2011. Controlling harmful cyanobacterial blooms in a world experiencing anthropogenic and climatic-induced change. Science of the Total Environment 409, 1739-1745.

Paerl, H.W., Huisman, J., 2008. Blooms like it hot. Science- New York then Washington 320, 57.

Paerl, H.W., Huisman, J., 2009. Climate change: a catalyst for global expansion of harmful cyanobacterial blooms. Environmental Microbiology Reports 1, 27-37.

Paerl, H.W., Paul, V.J., 2012. Climate change: links to global expansion of harmful cyanobacteria. Water research 46, 1349-1363.

Palmer, S.C.J., Kutser, T., Hunter, P.D., 2015a. Remote sensing of inland waters: Challenges, progress and future directions. Remote Sensing of Environment 157, 1-8.

Palmer, S.C.J., Odermatt, D., Hunter, P.D., Brockmann, C., Présing, M., Balzter, H., Tóth, V.R., 2015b. Satellite remote sensing of phytoplankton phenology in Lake Balaton using 10years of MERIS observations. Remote Sensing of Environment 158, 441-452.

Papenfus, M., Schaeffer, B., Pollard, A.I., Loftin, K., 2020. Exploring the potential value of satellite remote sensing to monitor chlorophyll-a for U.S. lakes and reservoirs. Environmental Monitoring and Assessment 192, 1-22.

Psilovikos, A., Margoni, S., Psilovikos, A., 2006. Simulation and trend analysis of the water quality monitoring daily data in Nestos River Delta. Contribution to the sustainable management and results for the years 2000-2002. Environ Monit Assess 116, 543-562.

R Core Team, 2015. R: A Language and Environment for Statistical Computing, Vienna, Austria.

Rogalus, M.K., Watzin, M.C., 2008. Evaluation of sampling and screening techniques for tiered monitoring of toxic cyanobacteria in lakes. Harmful Algae 7, 504-514.

Santhanam, H., Farooqui, A., Karthikeyan, A., 2018. Bloom of the diatom, Biddulphia sp. and ecology of Pulicat lagoon, Southeast India in the aftermath of the 2015 north east monsoonal rainfall. Environ Monit Assess 190, 636.

Santhanam, H., Majumdar, R., 2022. Quantification of green-blue ratios, impervious surface area and pace of urbanisation for sustainable management of urban lake – land zones in India -a case study from Bengaluru city. Journal of Urban Management.

Schaeffer, B.A., Bailey, S.W., Conmy, R.N., Galvin, M., Ignatius, A.R., Johnston, J.M., Keith, D.J., Lunetta, R.S., Parmar, R., Stumpf, R.P., Urquhart, E.A., Werdell, P.J., Wolfe, K., 2018. Mobile device application for monitoring cyanobacteria harmful algal blooms using Sentinel-3 satellite Ocean and Land Colour Instruments. Environmental Modelling & Software 109, 93-103.

Schaeffer, B.A., Loftin, K.A., Stumpf, R.P., Werdell, P.J., 2015. Agencies collaborate, develop a cyanobacteria assessment network. *EOS* 96.

Schellhammer, M., 2019. Harmful algae blooms detected in Allegheny Reservoir, Olean Times Herald. Community Media Group, LLc, New York.

Seegers, B.N., Werdell, P.J., Vandermeulen, R.A., Salls, W., Stumpf, R.P., Schaeffer, B.A., Owens, T.J., Bailey, S.W., Scott, J.P., Loftin, K.A., 2021. Satellites for long-term monitoring of inland U.S. lakes: the MERIS time series and application for chlorophyll a. Remote Sensing of Environment 266, 112685.

Sen, P.K., 1968. Estimates of the regression coefficient based on Kendall's tau. Journal of the American Statistical Association 63, 1379-1389.

Shi, K., Zhang, Y., Zhou, Y., Liu, X., Zhu, G., Qin, B., Gao, G., 2017. Long-term MODIS observations of cyanobacterial dynamics in Lake Taihu: Responses to nutrient enrichment and meteorological factors. Scientific reports 7, 40326.

Smayda, T.J., 1997. What is a bloom? A commentary. Limnol Oceanogr 42, 1132-1136.

Smith, N.J., Webster, K.E., Rodriguez, L.K., Cheruvelil, K.S., Soranno, P.A., 2021. LAGOS-US LOCUS v1.0: Data module of location, identifiers, and physical characteristics of lakes and their watersheds in the conterminous U.S. ver 1., in: Initiative, E.D. (Ed.), EDI Data Portal.

Soranno, P.A., Bissell, E.G., Cheruvelil, K.S., Christel, S.T., Collins, S.M., Fergus, C.E., Filstrup, C.T., Lapierre, J.F., Lottig, N.R., Oliver, S.K., Scott, C.E., Smith, N.J., Stopyak, S., Yuan, S., Bremigan, M.T., Downing, J.A., Gries, C., Henry, E.N., Skaff, N.K., Stanley, E.H., Stow, C.A., Tan, P.N., Wagner, T., Webster, K.E., 2015. Building a multi-scaled geospatial temporal ecology database from disparate data sources: fostering open science and data reuse. Gigascience 4, 28.

Stroming, S., Robertson, M., Mabee, B., Kuwayama, Y., Schaeffer, B., 2020. Quantifying the human health benefits of using satellite information to detect cyanobacterial harmful algal blooms and manage recreational advisories in U.S. lakes. GeoHelath, e2020GH000254.

Stumpf, R.P., Wynne, T.T., Baker, D.B., Fahnenstiel, G.L., 2012. Interannual variability of cyanobacterial blooms in Lake Erie. PLoS One 7, e42444.

Suter, G., 2007. II (2007) Ecological risk assessment. Boca Raton: CRC Press, Taylor and Francis Group.

Svirčev, Z., Tokodi, N., Drobac, D., 2017. Review of 130 years of research on cyanobacteria in aquatic ecosystems in Serbia presented in a Serbian Cyanobacterial Database. Advances in Oceanography and Limnology 8.

Taranu, Z.E., Gregory-Eaves, I., Leavitt, P.R., Bunting, L., Buchaca, T., Catalan, J., Domaizon, I., Guilizzoni, P., Lami, A., McGowan, S., Moorhouse, H., Morabito, G., Pick, F.R., Stevenson, M.A., Thompson, P.L., Vinebrooke, R.D., 2015. Acceleration of cyanobacterial dominance in north temperate-subarctic lakes during the Anthropocene. Ecology Letters 18, 375-384.

Theil, H., 1992. A Rank-Invariant Method of Linear and Polynomial Regression Analysis, in: Raj, B., Koerts, J. (Eds.), Henri Theil's Contributions to Economics and Econometrics: Econometric Theory and Methodology. Springer Netherlands, Dordrecht, pp. 345-381.

Tomlinson, M.C., Stumpf, R.P., Wynne, T.T., Dupuy, D., Burks, R., Hendrickson, J., Fulton Iii, R.S., 2016. Relating chlorophyll from cyanobacteria-dominated inland waters to a MERIS bloom index. Remote Sensing Letters 7, 141-149.

Urquhart, E.A., Schaeffer, B.A., 2020. Envisat MERIS and Sentinel-3 OLCI satellite lake biophysical water quality flag dataset for the contiguous United States. Data in Brief 28, 104826.

Urquhart, E.A., Schaeffer, B.A., Stumpf, R.P., Loftin, K.A., Werdell, P.J., 2017. A method for examining temporal changes in cyanobacterial harmful algal bloom spatial extent using satellite remote sensing. Harmful Algae 67, 144-152.

Utah DEQ, 2018a. Panguitch Lake Algal Bloom Monitoring 2018, Technical Report. Utah Department of Environmental Quality.

Utah DEQ, 2018b. Utah Lake Algal Bloom Monitoring 2018, Technical Report. Utah Department of Environmental Quality.

Verschuren, D., Johnson, T.C., Kling, H.J., Edgington, D.N., Leavitt, P.R., Brown, E.T., Talbot, M.R., Hecky, R.E., 2002. History and timing of human impact on Lake Victoria, East Africa. Proceedings of the Royal Society of London B: Biological Sciences 269, 289-294.

Whitman, P., Schaeffer, B., Salls, W., Coffer, M., Mishra, S., Seegers, B., Loftin, K., Stumpf, R., Werdell, P.J., In Press. A validation of satellite derived cyanobacteria detections with state reported events and recreation advisories across U.S. lakes. . Harmful Algae.

Wilcoxon, F., 1945. Individual Comparisons by Ranking Methods. Biometrics Bulletin 1.

Wilkinson, G.M., Walter, J.A., Buelo, C.D., Pace, M.L., 2021. No evidence of widespread algal bloom intensification in hundreds of lakes. Frontiers in Ecology and the Environment.

Winder, M., Cloern, J.E., 2010. The annual cycles of phytoplankton biomass. Philos Trans R Soc Lond B Biol Sci 365, 3215-3226.

Wynne, T., Meredith, A., Briggs, T., Litaker, W., Stumpf, R., 2018. Harmful algal bloom rorecasting branch ocean color satellite imagery processing guidelines. . NOAA Technical Memorandum NOS NCCOS 2018 252, 48.

Wynne, T.T., Mishra, S., Meredith, A., Litaker, R.W., Stumpf, R.P., 2021. Intercalibration of MERIS, MODIS, and OLCI Satellite Imagers for Construction of Past, Present, and Future Cyanobacterial Biomass Time Series. Remote Sensing 13.

Wynne, T.T., Stumpf, R.P., 2015. Spatial and temporal patterns in the seasonal distribution of toxic cyanobacteria in western lake erie from 2002–2014. Toxins 7, 1649-1663.

Wynne, T.T., Stumpf, R.P., Tomlinson, M.C., Dybleb, J., 2010. Characterizing a cyanobacterial bloom in western Lake Erie using satellite imagery and meteorological data. Limnology and Oceanography 55, 2025-2036.

Wynne, T.T., Stumpf, R.P., Tomlinson, M.C., Warner, R.A., Tester, P.A., Dyble, J., Fahnenstiel, G.L., 2008. Relating spectral shape to cyanobacterial blooms in the Laurentian Great Lakes. International Journal of Remote Sensing 29, 3665-3672.

Wyoming DEQ, 2018a. Big Sandy Reservoir harmful cyanobacterial investigation 2018, Technical Report. Wyoming Department of Environmental Quality.

Wyoming DEQ, 2018b. Eden Reservoir harmful cyanobacterial investigation 2018, Technical Report. Wyoming Department of Environmental Quality.

Wyoming DEQ, 2018c. Pathfinder Reservoir harmful cyanobacterial investigation 2018, Technical Report. Wyoming Department of Environmental Quality.

Wyoming DEQ, 2019a. Festo Lake: Harmful Cyanobacterial Bloom (HCB) Recreational Use Advisory, Technical Report. Wyoming Department of Environmental Quality.

Wyoming DEQ, 2019b. Flaming Gorge Reservoir: Harmful Cyanobacterial Bloom (HCB) Recreational Use Advisory, Technical Report. Wyoming Department of Environmental Quality.

Wyoming DEQ, 2019c. Fontenelle Reservoir: Harmful Cyanobacterial Bloom (HCB) Recreational Use Advisory, Technical Report. Wyoming Department of Environmental Quality.

Wyoming DEQ, 2019d. Harmful cyanobacterial bloom (HCB) recreational use advisories lifted at multiple waterbodies., Technical Report. Wyoming Department of Environmental Quality.

Wyoming DEQ, 2019e. Kemmerer City Reservoir: Harmful Cyanobacterial Bloom (HCB) Recreational Use Advisory, Technical Report. Wyoming Department of Environmental Quality.

Wyoming DEQ, 2019f. Keyhole Reservoir: Harmful Cyanobacterial Bloom (HCB) Recreational Use Advisory, Technical Report. Wyoming Department of Environmental Quality.

Wyoming DEQ, 2019g. Lake Viva Naughton: Harmful Cyanobacterial Bloom (HCB) Recreational Use Advisory, Technical Report. Wyoming Department of Environmental Quality.

Wyoming DEQ, 2019h. Woodruff Narrows Reservoir: Harmful Cyanobacterial Bloom (HCB) Recreational Use Advisory, Technical Report. Wyoming Department of Environmental Quality.

Xu, H., Paerl, H.W., Zhu, G., Qin, B., Hall, N.S., Zhu, M., 2017. Long-term nutrient trends and harmful cyanobacterial bloom potential in hypertrophic Lake Taihu, China. Hydrobiologia 787, 229-242.

Zhang, Y., Luo, P., Zhao, S., Kang, S., Wang, P., Zhou, M., Lyu, J., 2020. Control and remediation methods for eutrophic lakes in the past 30 years. Water Sci Technol 81, 1099-1113.